CHAPTER VI

THE AETHER DRIFT EXPERIMENT AND ASSOCIATED MEASUREMENTS

1. Introduction.

A substantial increase in the sensitivity of the aether drift experiment was achieved by maximizing the slope of the resonance, the counting rate, the duty cycle and the speed of the rotor. The inherent stability of the magnetic suspension also allowed for long continuous experimental runs and a straightforward analysis of the data.

In the particular geometry used in the experiment (see Figure 5.2) the source was mounted at the rim of the rotor and the absorber on the skirt near the center of the rotor. With the distance between the source and the absorber being 7.8 cm, the energy shift resulting from time dilatation is as shown in Figure 6.1. Given the knowledge of the operational velocities obtainable with the rotor, the appropriate source-absorber combinations could then be readily found.

2. Preparation of the Mössbauer Source and Absorber.

Table 1 gives the Mössbauer parameters for ^{57}Fe. As discussed in section 3.3.3, one would like to find a source with highest recoilless fraction and narrowest line width.

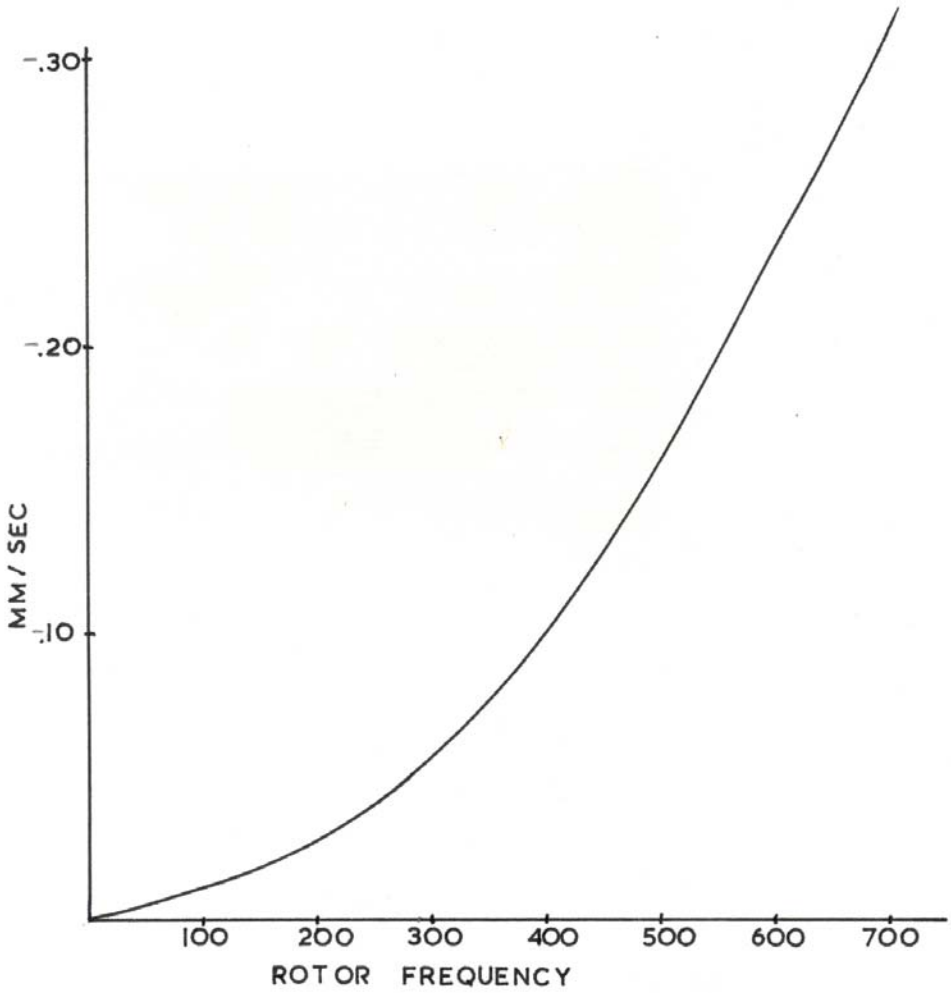

FIGURE 6.1

Table 6.2

Source lattice	ΔE_{IS} (mm/sec)	Γexp (mm/sec)	Absorber Used	Reference
Rh	-.114	0.29	S.F.C. [1] (Ta=1)	Qaim et al. (1967)
		0.34	S.F.C. (Ta=1.2)	Present experiment
		0.32	nat. iron (Ta=1)	Present experiment
Pd	-.185	0.31	S.F.C. (Ta=1)	Qaim et al. (1967)
		0.53	S.F.C. (Ta=1)	Present experiment
Cu	-.226	0.29	S.F.C. (Ta=1)	Qaim et al. (1967)
		0.29	P.F.C.[2]	Taylor et al. (1964)
		0.23	nat. iron	Taylor et al. (1964)
Mo	-.060	0.30	S.F.C. (Ta=1)	Qaim et al. (1967)
		0.28	nat. iron (Ta=0.28)	Qaim et al. (1967)

1) S.F.C. = $Na_4Fe(CN)_6$

2) P.F.C. = $K_4Fe(CN)_6$

Table 1

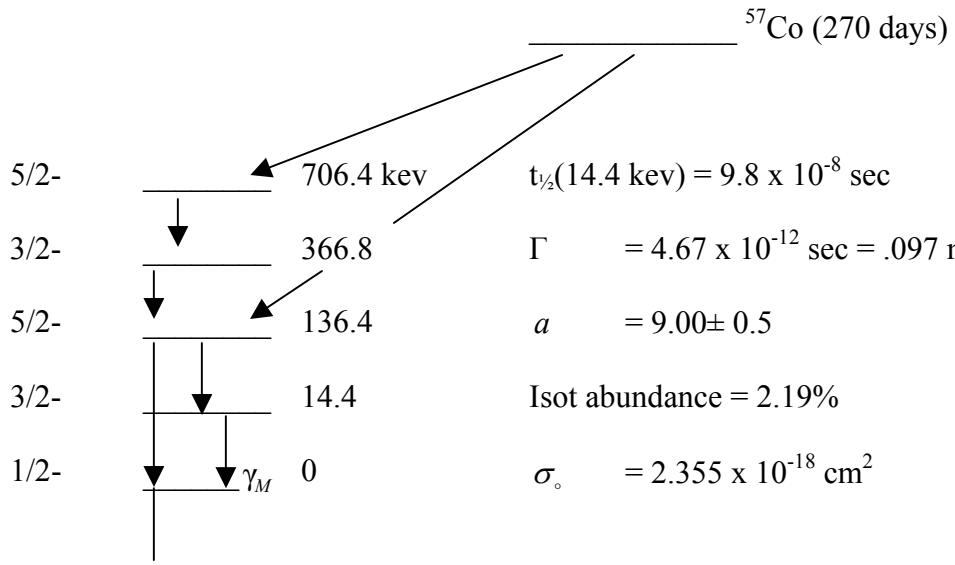

$t_{½}$(14.4 kev) = 9.8 x 10^{-8} sec

Γ = 4.67 x 10^{-12} sec = .097 mm/sec

a = 9.00± 0.5

Isot abundance = 2.19%

$\sigma_{\circ}$ = 2.355 x 10^{-18} cm^2

The values shown in Table 6.2 indicate that the line widths for the four source lattices with the highest f_s are nearly the same. The small differences in the line width are probably a result of the different techniques employed to produce the sources. For an identical $Na_4Fe(CN)_6$ absorber with T_a~1 the resultant line widths are typically .29 - .31 mm/sec. For natural line widths the expected width would be .22 mm/sec.

In the course of the experiment two sources were used. The first was a ^{57}Co in palladium source (10 mCi) with the active area measuring 1.3 x 9 mm. It exhibited an excessive line width of .56 mm/sec for a P.F.C. absorber with T_a = 2. In order to reduce the line width the source was reannealed at 1000°C (nominal) in a hydrogen atmosphere, and the radioactive surface was scraped to remove any surface impurities. This did not significantly improve the transmission line width. The excess line width can be partly attributed to the fact that the source, originally 116 mCi strong, exhibits an appreciable amount of self absorption (T_s ~ .8) which would broaden the emission line by

~ .03 mm/sec. A more general study (Evans, 1968) has also indicated that old sources can be broadened by as much as Γ which would explain the excess line width.

The other source used consisted of ^{57}Co in rhodium with an initial source strength of 50 mCi and a radioactive area of 1.3 x 11 mm. This source was also reannealed, at 1200°C, and then cut to size to fit the rim of the rotor.

The final parameters of the two sources relative to a (T_a = 2) S.F.C. absorber are given in table 6.3.

Table 6.3

Source	Γ_{exp} (mm/sec)	E_{IS} (mm/sec)	R_m
^{57}Co(Pd)	.535 ± .015	-.229 ± .005	.55 ± .015
^{57}Co(Rh)	.350 ± 0.008	-.155 ± .005	.70 ± .020

The negative sign of the energy shift implies that the transition energy of the source is larger than that of the absorber, so that the shift resulting from the time dilatation factor would sweep the emission line over the absorption line.

This means that a ^{57}Co(Pd) source used with a S.F.C. absorber is an ideal combination for rotor frequencies up to 450 cps, while a ^{57}Co(Rh) source with a S.F.C. absorber is ideal for frequencies above 625 cps. The rotor frequency corresponding to the optimum slope depended on the characteristics of the individual absorbers.

Three different absorbers were used all made from S.F.C. enriched to 91% in ^{57}Fe. To make the absorbers more stable under high temperatures the crystals of $Na_4Fe(CN)_6.10H_20$ were dehydrated and then cast in araldite. The dehydration occurred in several stages by heating the crystals to 130°C until a constant weight was obtained. The weight difference accounted for 95% of the water of hydration, which suggested that

the crystals had already been partially dehydrated. The S.F.C. was then ground to a fine powder, mixed with araldite in the ratio of 1:7 and allowed to harden between two sheets of polythene, which were spaced to give the desirable thickness of $T_a = 4$. The absorbers prepared in this way were mechanically very strong and could withstand temperatures of up to 130°C.

The first two absorbers made had an ^{57}Fe concentration of .84 mg/cm^2 and .395 mg/cm^2 respectively. Because of the high concentration of ^{57}Fe only a small amount of S.F.C. was needed to give the desirable absorber thickness. This turned out to be a disadvantage as the absorbers ended up being not very uniform and exhibited a grainy texture. This resulted in a smaller R_m value than expected. For that reason the thinner absorber, which had an effective area of 25.6 cm^2, was cut in half and doubled in thickness. All three of these absorbers were used during the experiment and will be denoted as absorbers 1, 2, 3.

Absorber 1 was used with the palladium source and the steel absorber skirt. It was mounted onto two .008" thick beryllium discs and then fitted into the recessed window of the steel skirt. Absorbers 2 and 3 were used with the rhodium source and the beryllium skirt. They were directly glued to the inside of the skirt so as to cover all of the detector area as seen by the source. Outside of the tantalum collimator, which shielded the lower unused portion of the counter, no collimation was used.

Because of the non-uniformity of the absorber and the resonant absorption in the beryllium skirt (see Figure 6.5) it as not possible to obtain accurate line width measurements until the absorber was finally mounted on the rotor. This produced other difficulties as the geometry using the rotor and the central proportional counter was not as

well defined as in a bench experiment. The higher vibration level of the rotor structure, used to support the counting equipment, added additional uncertainty to the results. Hence for the final accurate evaluation of the data the slope of the resonance at the operating speeds of the rotor was determined directly from the change in the counting rates observed during the acceleration of the rotor, (see Section 6.10) after allowing it to cool.

Figures 6.2, 6.3 and 6.4 show the transmission spectra for the three source-absorber combinations. The spectra were taken with the absorber mounted as during an actual experiment. The source was attached to the vibrator, which was inclined to approximate the position of the source as when it is mounted on the rotor. The central proportional counter was shielded against the source radiation, which did not penetrate the absorber. Figure 6.2 indicates the excessive line width of the ^{57}Co (Pd) source. The slope of the resonance is maximum at rotor frequencies of 300 and 800 cps and zero at 600 cps. Figures 6.3 and 6.4 show that the transmission line width is not broadened very much by doubling the thickness of the absorber, which further indicates the non uniformity of the absorber. The R_m value, however, was almost doubled. The slope is maximum for frequencies of 225 and 670 cps and minimum at 495 cps. In the final series of runs the rotor was run at 650 and 701 cps from which the slope at the inflection point was found as being 2.28×10^{11}.

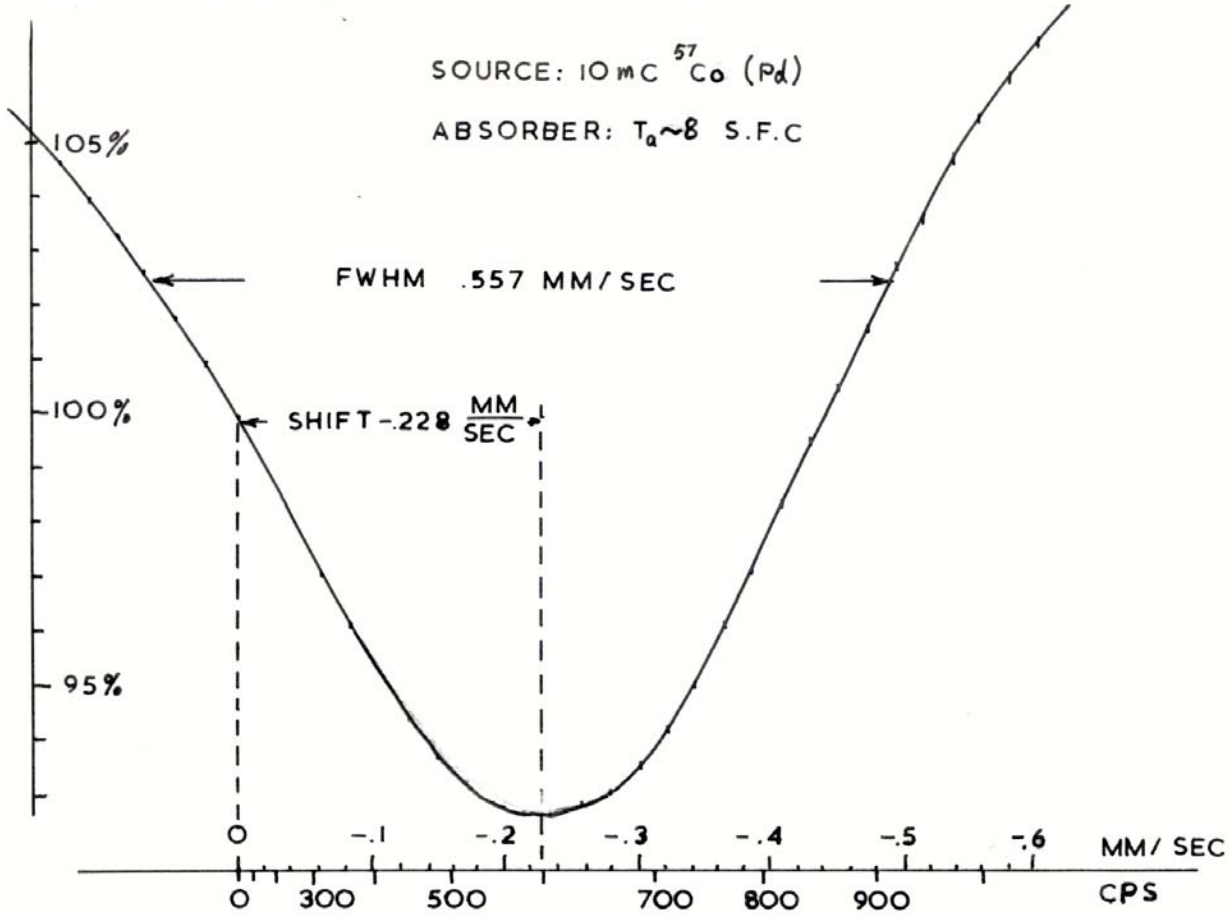
SOURCE: 10 mC 57Co (Pd)
ABSORBER: Ta~8 S.F.C
105%
100%
95%
FWHM .557 MM/SEC
SHIFT -.228 MM/SEC
0
-.1
-.2
-.3
-.4
-.5
-.6
MM/SEC
0
300
500
700
800
900
CPS

FIGURE 6.2

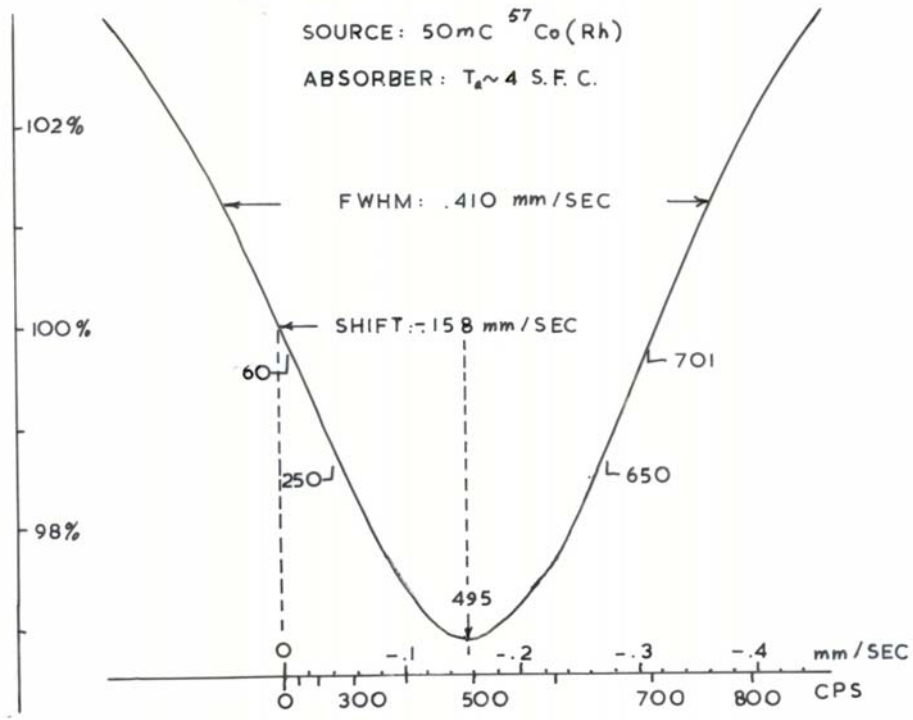
SOURCE: 50mC 57Co(Rh)
ABSORBER: Ta~4 S.F.C.
102%
100%
98%
FWHM: .410 mm/SEC
SHIFT: -.158 mm/SEC
60
250
701
650
495
0
-.1
-.2
-.3
-.4
mm/SEC
0
300
500
700
800
CPS

FIGURE 6.3

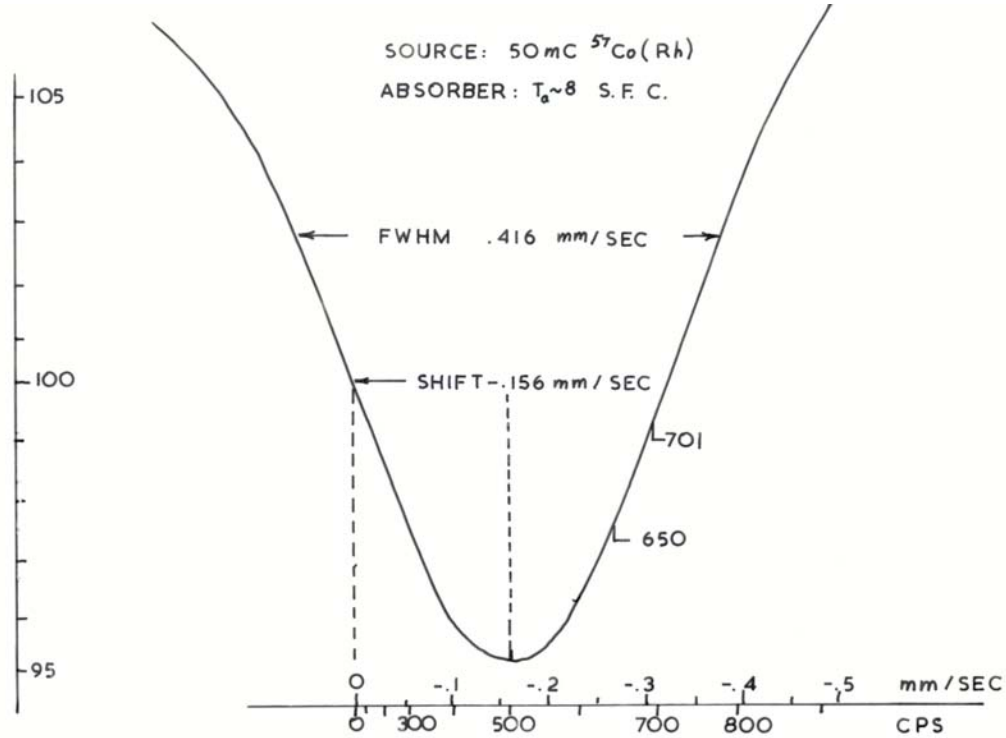
SOURCE: 50 mC ^{57}Co(Rh)
ABSORBER: T_a~8 S.F.C.
FWHM .416 mm/SEC
SHIFT -.156 mm/SEC
105
100
95
701
650
0
-.1
-.2
-.3
-.4
-.5
mm/SEC
0
300
500
700
800
CPS

FIGURE 6.4

In order to determine the iron content in the beryllium another spectrum was taken using beryllium tubing 4 mm thick (see Figure 6.5). The spectrum shows that even though the beryllium is 99.9% pure it contains enough iron to produce a ~1% resonance dip for every 1 mm thickness of beryllium. The transmission line is quadrupole split and very broad (.83 mm/sec) so that the resulting transmission line width, when using the S.F.C. absorber and the 2 mm thick beryllium skirt, would be slightly increased.

To establish the effect of the graininess of the absorbers another series of spectra was taken using the ^{57}Co(Rh) source and a set of unenriched S.F.C. absorbers (supplied by M. J. Evans). The absorbers were quite uniform and ranged in thickness from .05 to .47 mg/cm^2 of ^{57}Fe. The line widths and R_m values obtained are shown in Figures 6.6 and 6.7. Figure 6.6 is plotted as a function of $N\sigma_\circ$, where N is the number of resonant nuclei per cm^2, such that the slope is equal to 0.27 f_a. As drawn $f_a = .40 \pm .05$. Superimposed on the graph are the line widths obtained using the same source and natural iron foil absorbers. Extrapolating the line widths data to zero absorber thickness it appears that the iron foil absorbers give a line width narrower by .02 mm/sec than those obtained for the S.F.C. absorber. If one assumes that the absorption line of iron is natural one obtains for the ^{57}CO (Rh) source a width $\Gamma_e \approx 2.1\Gamma$ or $k_s \approx 0.5$ (see § 3.3.3). This means that the slope of the resonance using an unenriched S.F.C. absorber with $T_a = 4$ is .48 of the slope obtained with unbroadened lines. In Figure 6.7, the experimental R_m values are compared with the theoretically expected values assuming $f_s = .7$.

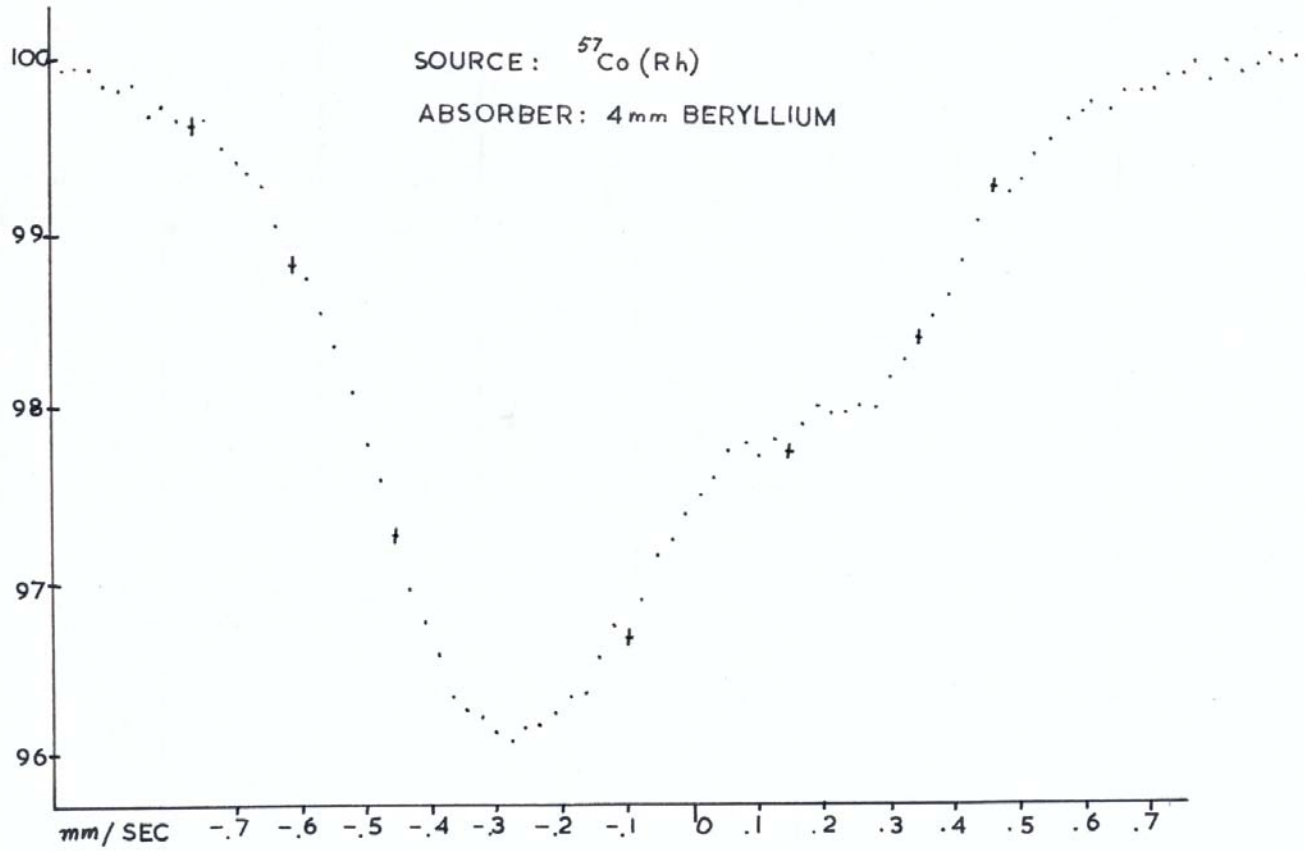
SOURCE: 57Co (Rh)
ABSORBER: 4mm BERYLLIUM
100
99
98
97
96
mm/SEC
-.7 -.6 -.5 -.4 -.3 -.2 -.1 0 .1 .2 .3 .4 .5 .6 .7

FIGURE 6.5

The effective thickness of the three absorbers can then be deduced by comparing the observed transmission spectra, using the same ^{57}Co (Rh) source, with the values of the unenriched absorbers. The parameters of the three absorbers are shown in Table 6.4.

Table 6.4

Absorber	mg/cm^2 of ^{57}Fe	nominal T_a	Γ exp mm/sec	R_m
1	.84 mg/cm^2	8.3	.424	.209
2	.395 mg/cm^2	3.9	.410	.110
3	.79 mg/cm^2	7.8	.416	.214

The values of Γ_{exp} and R_m for absorbers 1 and 3 have been superimposed on Figure 6.6 and 6.7. This shows that even though the two absorbers have a nominal thickness of T_a = 8.3 and 7.8 respectively, the observed line widths are rather narrower than expected and in fact are representative of T_a = 3.5 and 3.2 respectively. Similarly, the observed R_m values are smaller and give T_a values of 1.75 and 1.8. This means that the slopes obtained with absorbers 1 and 3 are .32 and .33 of the slope for the ideal case. This was still considered tolerable as the electronic absorption for these absorbers is also smaller than for the unenriched absorbers.

In order to correlate the spectra obtained using the linear Doppler shift with those obtained with the time dilatation shift, the background counting rates had to be known accurately. For the rotor experiment the background was measured, while the rotor was

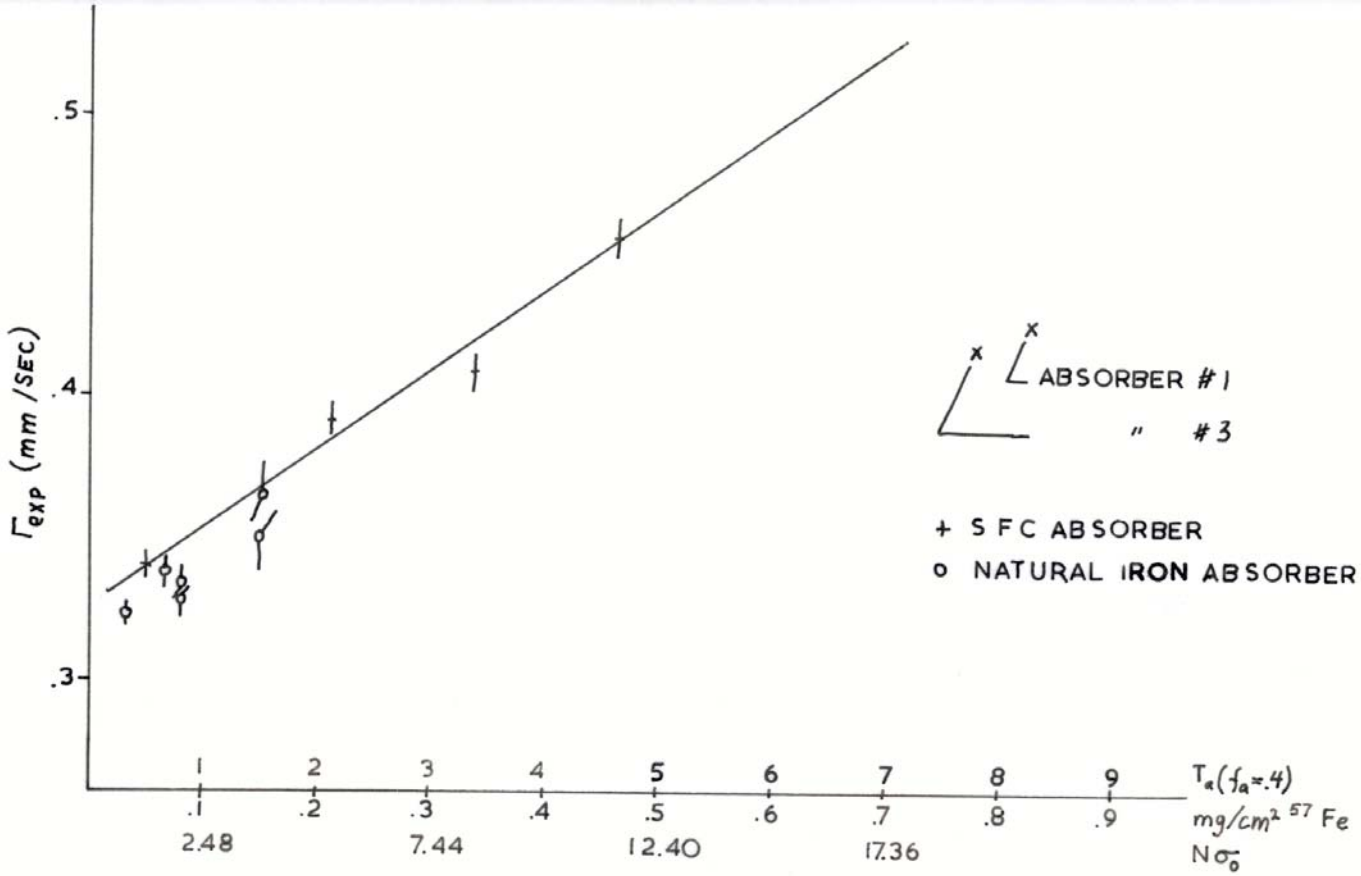
.5
.4
.3
Γ_{exp} (mm /SEC)
ABSORBER #1
" #3
+ S F C ABSORBER
o NATURAL IRON ABSORBER
1 2 3 4 5 6 7 8 9
.1 .2 .3 .4 .5 .6 .7 .8 .9
2.48 7.44 12.40 17.36
$T_a(f_a=.4)$
mg/cm² ^{57}Fe
$N\sigma_0$

FIGURE 6.6

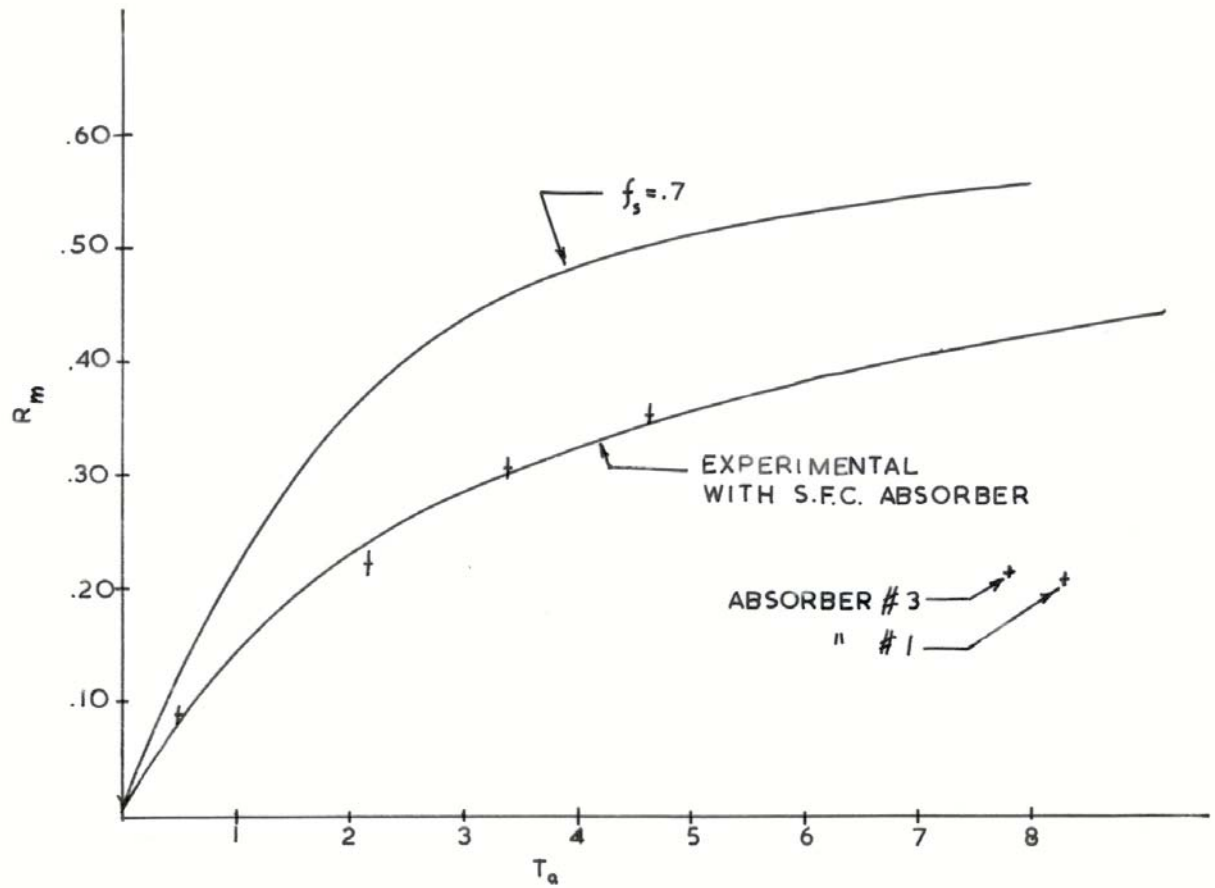
.60
.50
.40
.30
.20
.10
R_m
$f_s = .7$
EXPERIMENTAL
WITH S.F.C. ABSORBER
ABSORBER # 3
" # 1
1
2
3
4
5
6
7
8
T_a

FIGURE 6.7

not suspended by interposing two 1/16" thick aluminum sheets between the skirt and the detector. Because this geometry is not identical to the one when the rotor is actually suspended, the measurement is not very accurate, so that the experiment cannot be considered to be a very sensitive test of time dilatation.

The temperature dependence of the counting rate, with the source and the absorber both mounted on the rotor, was measured by using the rotating magnetic field to heat the stationary rotor to a temperature of 120°C. With the rotor kept in the vacuum the temperature was monitored with a copper-constantan thermocouple. The increase in the counting rate resulting from the decrease in f_s and f_a amounted to (.15 ± .01)% per °C and served as a rough indication of the rotor temperature.

3. Gamma Ray Detector.

Several methods of detection were considered including

i) scintillation counter,

ii) ionization chamber, and

iii) proportional counter.

The detector had to have a high resolution so as to resolve the 14.4 kev gamma ray peak or at least have a high detection efficiency for that peak to reduce the background level. It also had to have a fast response time and be insensitive to stray magnetic fields and strong enough to support the rotor.

i) A scintillation counter, even though it had a potentially unit detection efficiency for the 14.4 kev peak, was ruled out because it failed to satisfy most of the other criteria. In order to make the detector insensitive to the high energy gamma radiation it would have

had to be a thin annular ring (~1 mm wall thickness), which would have made the counter structurally very weak. The resolution of a scintillation crystal (NaI) even under best conditions is poorer than that of a proportional counter with typical resolutions of 30% and 15% respectively for 14.4 kev radiation. The need of a photomultiplier makes such a detection system very sensitive to stray magnetic fields.

ii) An ionization chamber has been suggested for the use in conjunction with strong sources (Isaak, 1965) as it measures currents rather than individual pulses. Filling the chamber with a krypton-methane gas mixture would result in a high detection efficiency for the 14.4 kev radiation, because the K-absorption edge of krypton is at 14.3 kev. This means that the high energy gamma rays (136 and 122) would be rejected in a ratio of 350:1. As the ionization chamber does not discriminate against the pulses this rejection ratio and a suitable absorber material could reduce the background level to less than half of the total signal level. The technical problem in the present situation, however, is that the ammeter measuring the ionization current would have had to have a 1 ms response time to cope with the fast rotor modulation, and no such instrument is as yet available.

iii) For these reasons a proportional counter was the most promising choice, even though several problems had first to be solved. The counter had to have a small volume to fit inside the absorber skirt and at the same time had to retain a high counting efficiency constant to within 1% over a full revolution of the rotor.

Figure 6.8 shows the final design of the counter. Several have been built incorporating a beryllium tube of 1" diameter and a 1 mm (or 2mm) wall thickness to minimize electronic absorption. The glass to metal seals were selected to have a

PROPORTIONAL COUNTER

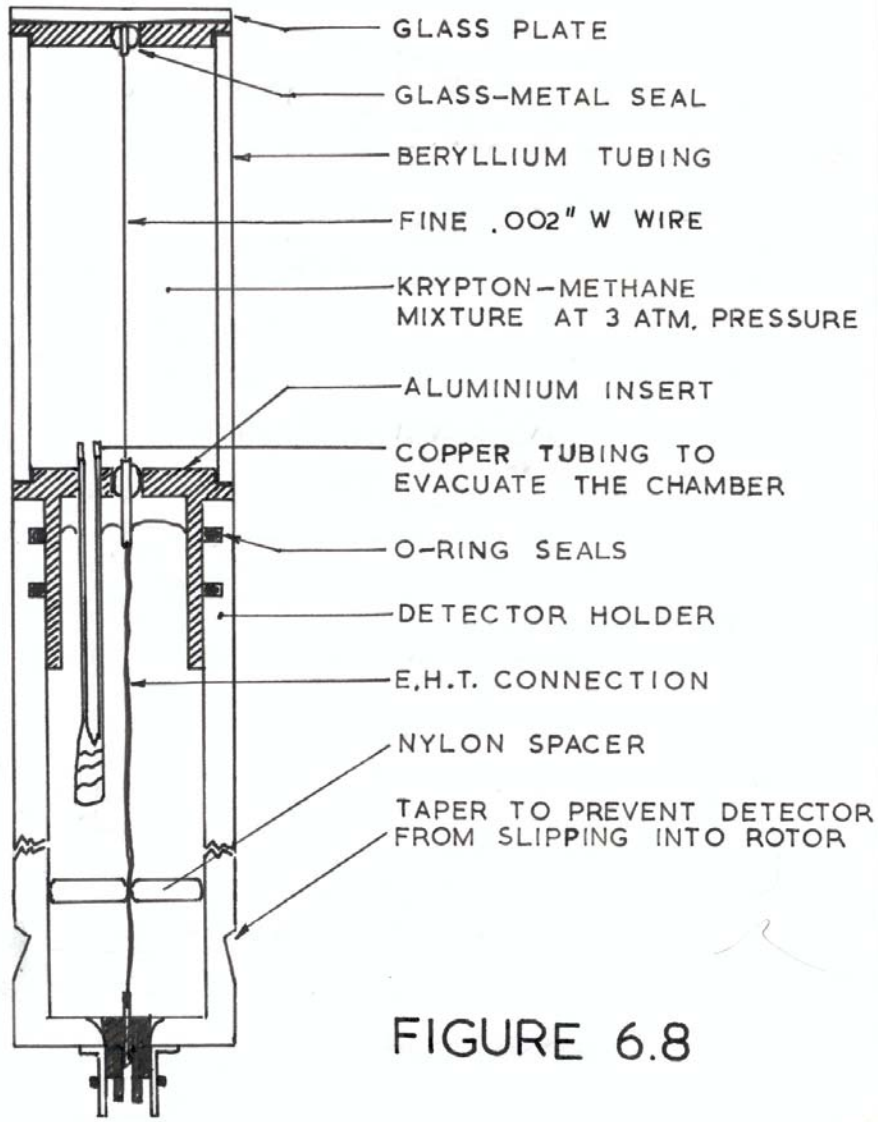

Multiplication constant if

$\frac{V}{\ln b/a}$ constant

V = applied voltage
b = outer radius
a = wire radius

FIGURE 6.8

resistance of greater than 10^{11} ohm to keep the noise level of the counter at a minimum. The beryllium was etched and the system assembled using araldite.

A ¼" copper tubing was used to evacuate the chamber over a period of a few weeks, while the walls were heated to a temperature of 100°C to increase the rate of outgassing. The counter was then flushed out several times using the 90% krypton; 10% methane mixture with which the counter was finally filled to a pressure of 2-3 atmospheres.

Two 'O'-rings in the detector holder provided an effective vacuum seal and also, with three Allen screws, positioned the proportional counter. This assembly was inserted into the rotating vacuum seal at the center of the lower vacuum plate (see Figure 5.1) and a tapered groove in the detector holder prevented the proportional counter from slipping into the vacuum chamber. An agate disc was araldited to the top of the counter to support the rotor when not suspended and in case of emergency.

3.1 Proportional Counter Response.

This design proved to be very satisfactory. The resolution of various segments of the counter is shown in Figure 6.9. The pulse height spectrum 1 was taken with a circular collimator of 1 cm diameter restricting the beam to the central portion of the detector. The resolution for the 14.4 kev peak is 16%. Spectra 2 and 3 were taken with the collimator moved towards the top of the detector and, as expected, they indicate the presence of end effects, which distort the spectra. This was tolerable, however, as the detection efficiency decreased as well.

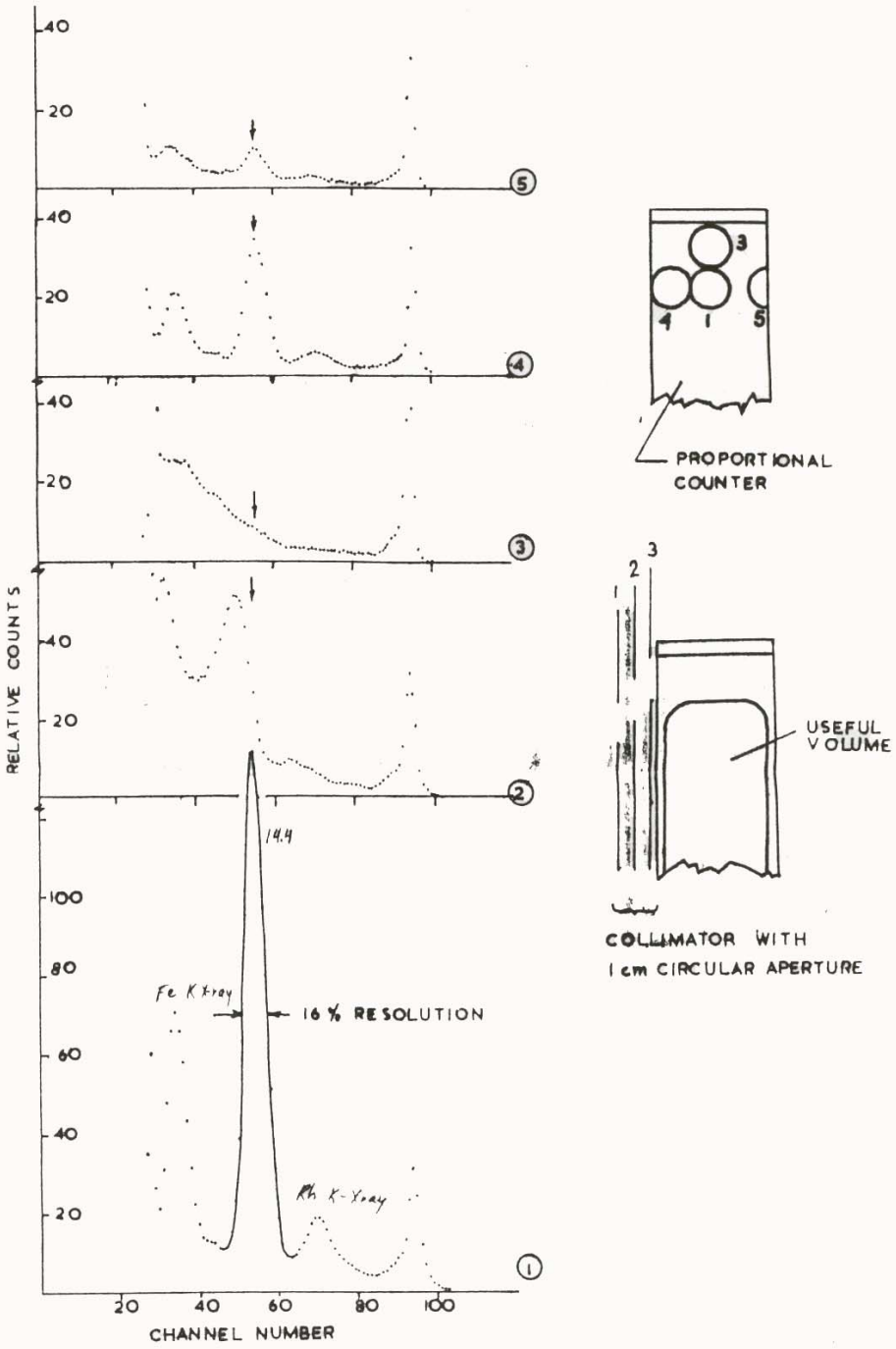
RELATIVE COUNTS
CHANNEL NUMBER
14.4
Fe K-Xray
16 % RESOLUTION
Rh K-Xray
PROPORTIONAL COUNTER
USEFUL VOLUME
COLLIMATOR WITH 1 cm CIRCULAR APERTURE

FIGURE 6.9

Spectra 4 and 5 exhibit the detector response with the collimator moved to the side of the counter. The peaks are still in the same position but the detection efficiency has decreased. The overall resolution using no collimator is 20%, which is good enough to resolve the 14.4 keV peak during the high speed run when the beryllium skirt is used.

The dependence of the counting rate on the horizontal position of the rotor, with the system as finally assembled, was measured by displacing the rotor along the two axes of the damping springs. The change in the counting rate amounted to (.96 ± .08)% per 1 mm displacement of the rotor and was the same within experimental error for both of the absorber skirts. Later measurements indicated that the horizontal position of the rotor was stable to within .02 mm over a period of one week.

The counting rate dependence on height was measured by varying the vertical position of the rotor over a range of ~2 mm, i.e., by changing the supply current by .5 amp. This caused a change in the counting rate of .105% per .1 amp change in the supply current. The counting rate also depended to some extent on the position of the tantalum collimator, which was used to shield the lower half of the proportional counter from the source radiation. As the angular asymmetry of the counting rate could be expected to depend on the height of the rotor, the suspension current was kept constant to within .02 Amp over 24 hours.

3.2 Efficiency of the Proportional Counter.

The efficiency of the first detector made was 24%, and was measured by comparing its counting rate with that of a scintillation counter assumed to have a 100%

efficiency. This low efficiency is partially caused by the electronic absorption in the 2 mm thick beryllium tubing (19%) and the finite absorption in the krypton-methane gas mixture (53%) for the relatively low gas pressures (1-2 atm) used in the first counter. The exact gas pressure could not be accurately assessed as it depended on the absorption and leakage of the gas in the counter, which were not known. It was also found that only 50% of the radiation absorbed by the counter did appear under the 14.4 keV peak which was attributed to the escape of the 12.6 keV krypton K X-ray. This was substantiated by the size of the escape peak at 1.8 keV, which was of comparable magnitude to the 14.4 keV peak (see Figure 6.11).

In the later counters a thinner beryllium tubing (1 mm thick) and higher gas pressures (2-3 atmospheres) were used, which increased the detection efficiency to ~35%.

4. Counter Electronics and Saturation Effects.

Even though the response of the various proportional counters was very similar, the voltages needed to give a satisfactory resolution varied from 1550 to 1700 volts and also depended partially on the noise level of the preamplifier (Nuclear Enterprises N.E. 5282) which was adjusted to have a gain of 18. The output of the preamplifier was further amplified and shaped by an Ortec 410 linear amplifier and then analyzed by a Hamner pulse height analyzer model NC-14A.

To determine the effect of high counting rates the resolution of the whole detection system was measured, as a function of the distance r between the uncollimated source and the detector, using the PHA of the 128 channel RCL kicksorter. The spectra shown in Figure 6.10 were taken with the 50 mCi strong ^{57}Co (Rh) source. They indicate

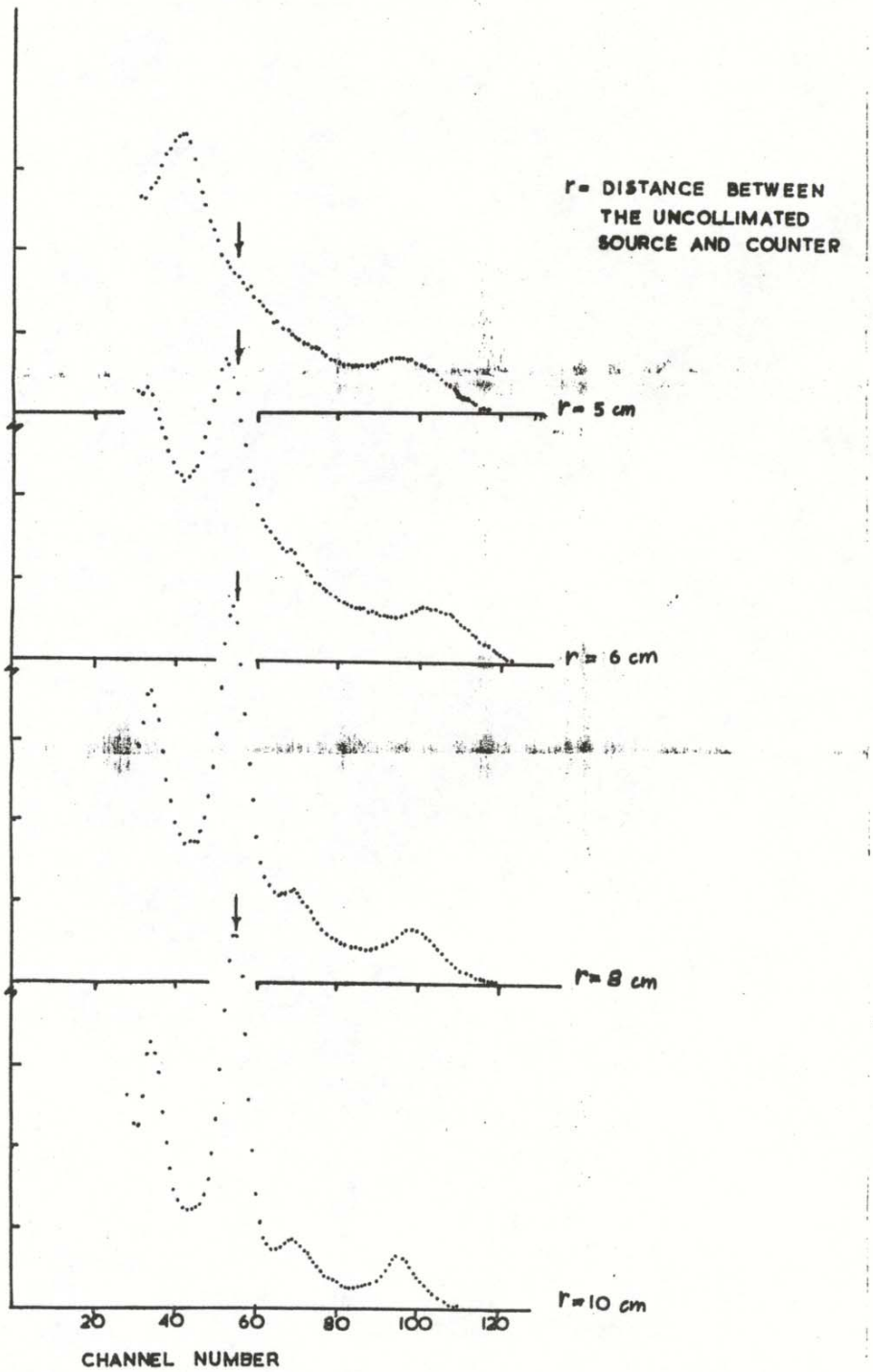
r= DISTANCE BETWEEN
THE UNCOLLIMATED
SOURCE AND COUNTER
r= 5 cm
r= 6 cm
r= 8 cm
r=10 cm
20
40
60
80
100
120
CHANNEL NUMBER

FIGURE 6.10

a definite deterioration in the resolution for r<8 cm. This shows that there would be no saturation for the source-detector distance of 10 cm actually used in the rotor experiment. As part of the distortion in the spectra can be attributed to the kicksorter another set of measurements was taken using the Hammer PHA with the energy window set on the 14.4 keV peak. The ration of the direct counting rate $\dot{N}_1$ and that $\dot{N}_2$ after interposing a .03 cm thick aluminum sheet, which halved the counting rate, was measured as a function of $\dot{N}_1$. It was found that $\dot{N}_1 / \dot{N}_2$ stayed constant up to $\dot{N}_1$ = 60,000 cts/sec, which indicates that for smaller counting rates the electronics can be assumed to have a linear counting rate response.

It would have been interesting to examine if this saturation is a result of the detector or of the electronics, but this could not be easily done without faster electronics and a random pulse generator, which were not available. The specifications of the amplifier suggest, however, that it is due to the amplifier becoming saturated at these counting rates.

The Ortec amplifier was used in the double delay line shaping mode, which considerably improved the resolution compared with the single delay line and RC shaping modes (see Figure 6.11). The gain of the amplifier was adjusted to make the peak to valley ration P_1/V_1 comparable with P_2/V_2, where P_1 and P_2 are the 14.4 keV peak and that caused by the limiting of the amplifier respectively. The levels of the PHA were set according to the criterion $\dot{N}_1 V_1 = \dot{N}_2 V_2$, so that small gain shifts would not appreciably change the counting rate. $\dot{N}_1$ and $\dot{N}_2$ are here the counting rates at V_1 and V_2. Furthermore, the EHT supply to the detector was adjusted to give, for the final setting of the PHA, a maximum counting rate. The overall stability of the counting rate during an

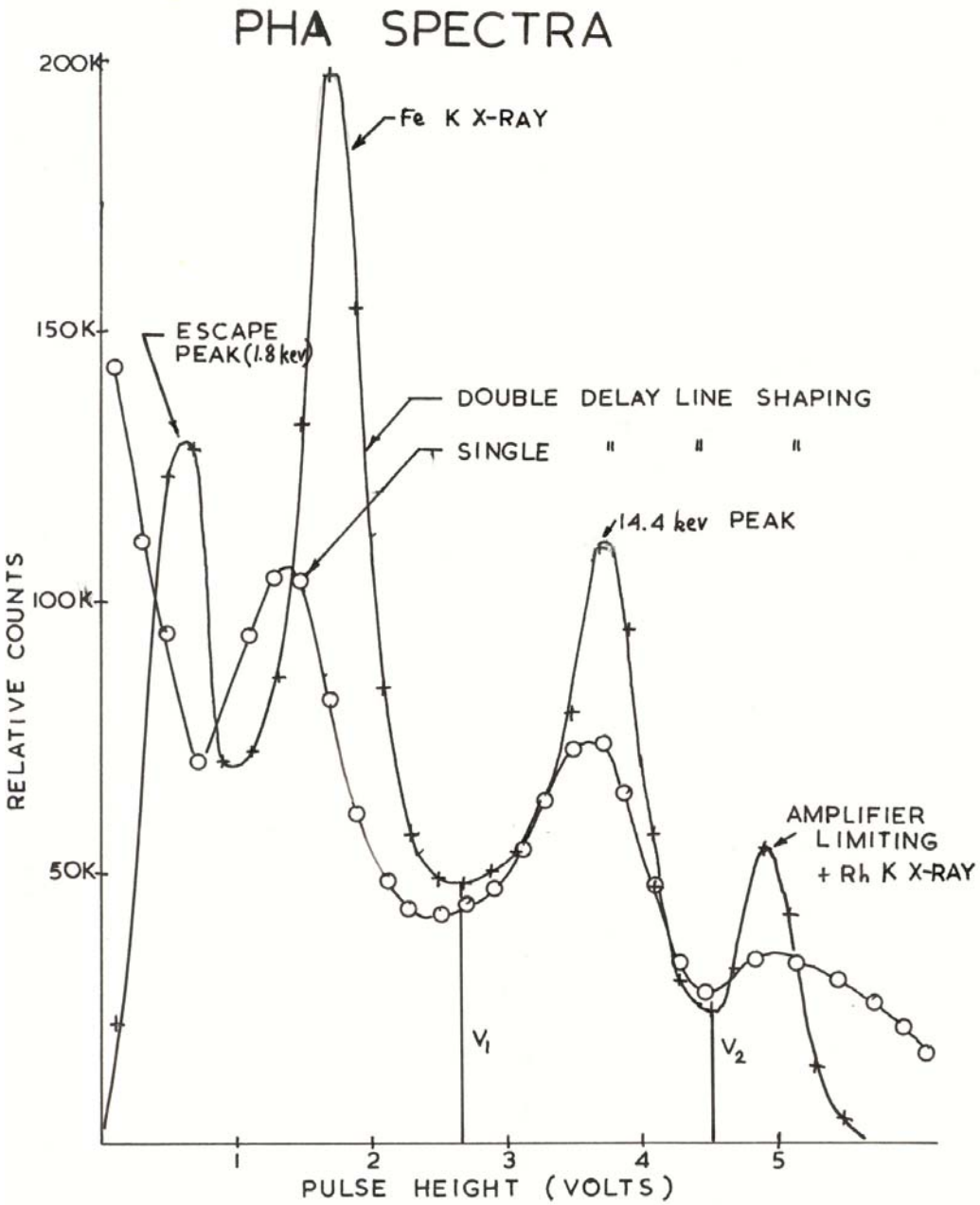
PHA SPECTRA
200K
150K
100K
50K
RELATIVE COUNTS
Fe K X-RAY
ESCAPE PEAK (1.8 kev)
DOUBLE DELAY LINE SHAPING
SINGLE " " "
14.4 kev PEAK
AMPLIFIER LIMITING + Rh K X-RAY
V1
V2
1
2
3
4
5
PULSE HEIGHT (VOLTS)

FIGURE 6.11

actual rotor run was then found to be remarkably constant. Figure 6.12 shows the counts accumulated during a four day rotor run at 701 eps, each point representing a 85 min. measurement. The slope represents the .257% decay of the source per day. The larger initial counting rate is a result of the rotor heating during acceleration.

5. Principle of Operation.

Figure 6.13 is a diagram of the principal layout of the electronics. The light beam S reflected off a polished strip at the lower surface of the rotor was detected by a photomultiplier tube, the output of which was shaped to give a 12-volt 2 μsec long pulse ST. This served as a starting signal for the kicksorter sweep and, in conjunction with a 5245 HP electronic counter, as an accurate monitor of the rotor speed.

The output of the PHA went directly into the kicksorter or, as in the last stage of the experiment, via a by-4 dividing network. The kicksorter had been modified to run on a 16 channel sweep with the time spent per channel determined by an external multivibrator which could be adjusted so that $(16+\varepsilon)$ channels corresponded to one revolution of the rotor. ε amounted to ~7% of the sweep cycle, which was needed to allow the kicksorter to recover for a new starting pulse.

The kicksorter starting pulse KST was derived from a logic circuit, which required the simultaneous presence of the ST pulse, the OVERFLOW and the $\overline{\text{OPERATE}}$ bias levels from the kicksorter. These levels indicated when the kicksorter had truly come to the end of its sweep.

To allow for a double check of the total counts accumulated a scaler with 1 μsec response time was used to count the PHA output. This scaler as well as the kicksorter

STABILITY OF COUNTING RATE

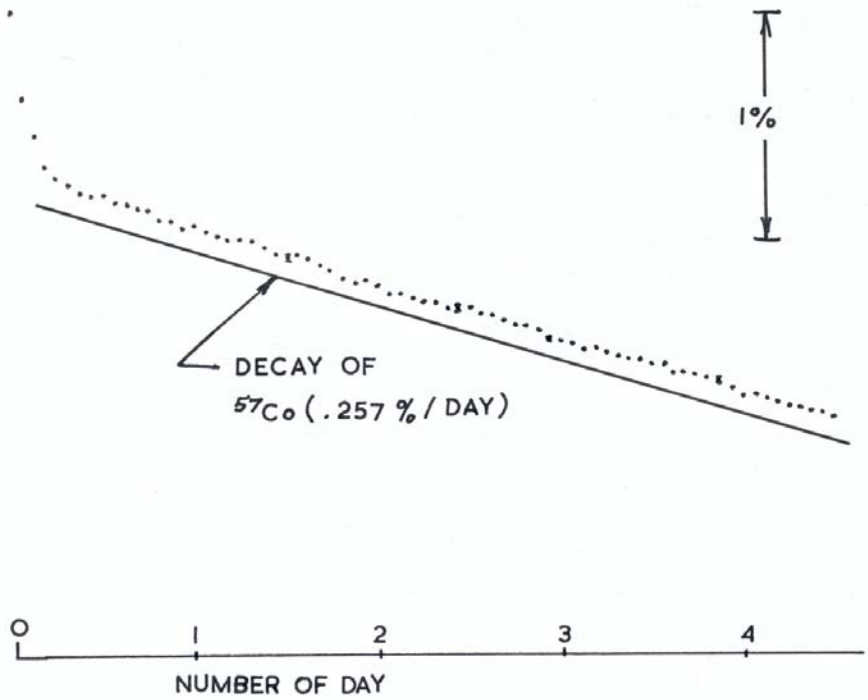

FIGURE 6.12

and two other scalers, the function of which will be discussed below, were gated by a manually controlled starting switch. A time scaler, counting at 10 cps, determined the total time spent per run.

The following parameters were also continuously monitored throughout the experiment: the ± 24 volt and ± 12 volt bias supplies, the temperatures of the rotor structure, the PHA, and the kicksorter. They were measured by converting the DC levels into frequencies which could be directly monitored by the HP frequency counter. At the later stages of the experiment the suspension current was also monitored because the visual display was not sufficiently accurate. These efforts proved to be worthwhile, as a number of anomalies in the counting rate could be readily traced to faulty bias supplies and be repaired without decelerating the rotor. The temperature measurements helped in the attempts to minimize electronic drifts, and an accurate monitoring of the suspension current was needed to eliminate the prime cause of a changing counting rate, i.e., a change in the rotor height. The resulting stability of the counting system was as shown in Figure 6.12.

6. Kicksorter Accumulation.

Even though 16 channels were used in the kicksorter only 14 could actually be used in the analysis. The first channel was the clock channel for other modes of operation and could not be easily altered to accept PHA pulses.

The second channel was lost because the channel advance multivibrator CAM was not synchronized with the rotor with the result that the slowing down of the rotor to the extent of .1% per run was not adjusted for. Also, the arrival of a CAM pulse during

an accumulation cycle would delay the channel advance by a few microseconds, which produced a channel jitter. To avoid missing a KST pulse the CAM rate had to be adjusted so that there was on average a time delay of 7% (of total sweep time) between sweeps.

Attempts were made to synchronize the CAM rate with the rotor frequency but these were not successful because the channel jitter made it impossible to obtain a useful correction signal.

To determine accurately what fraction of the sweep cycle was missed two scalers counting 10 cps clock pulses were gated by the OVERFLOW and the $\overline{\text{OPERATE}}$ levels respectively (see Figure 6.13).

The kicksorter had provisions to count a number of clock pulses before advancing one channel. In our system every CAM pulse advanced the channel and so this provision of a comparator network produced only unnecessary dead time in the kicksorter. Eliminating this logic circuit reduced the time needed to advance one channel from 20 to 13 μsec, i.e., reduced the dead time at a rotor frequency of 700 cps from 21% to 13.6% (see Figure 6.14).

7. Dead Time Effects.

For the later analysis of the data it is essential that one understands the effect of the dead times occurring at the various stages of the accumulation cycle as large counting rates can give rise to saturation effects producing a non-linear response to changes in the counting rate.

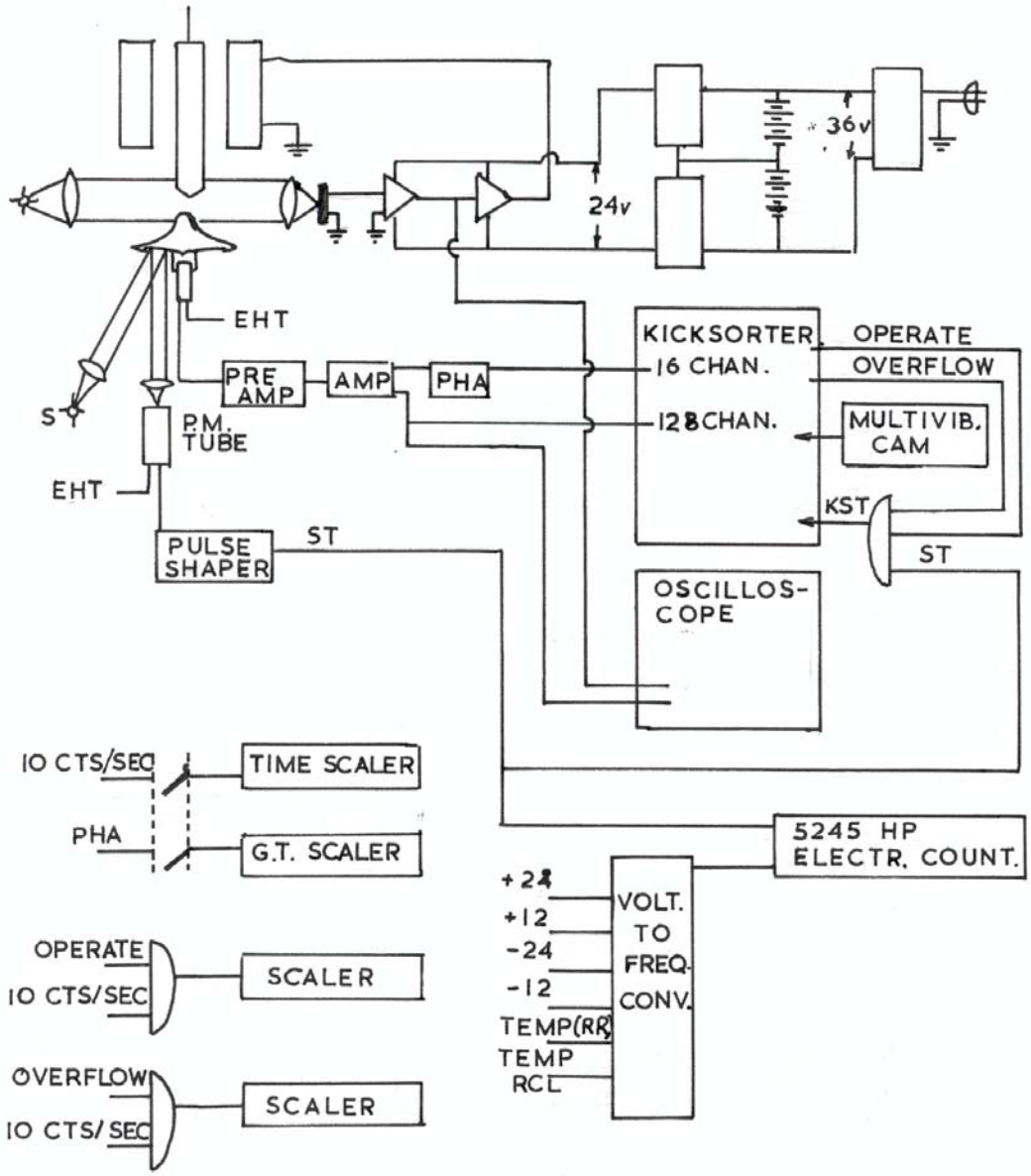
36v
24v
EHT
KICKSORTER
OPERATE
16 CHAN.
OVERFLOW
PRE AMP
AMP
PHA
128 CHAN.
MULTIVIB. CAM
S
P.M. TUBE
EHT
KST
ST
PULSE SHAPER
ST
OSCILLOS-COPE
10 CTS/SEC
TIME SCALER
PHA
G.T. SCALER
5245 HP ELECTR. COUNT.
+24
+12
-24
-12
TEMP(RR)
TEMP RCL
VOLT. TO FREQ. CONV.
OPERATE
10 CTS/SEC
SCALER
OVERFLOW
10 CTS/SEC
SCALER

FIGURE 6.13

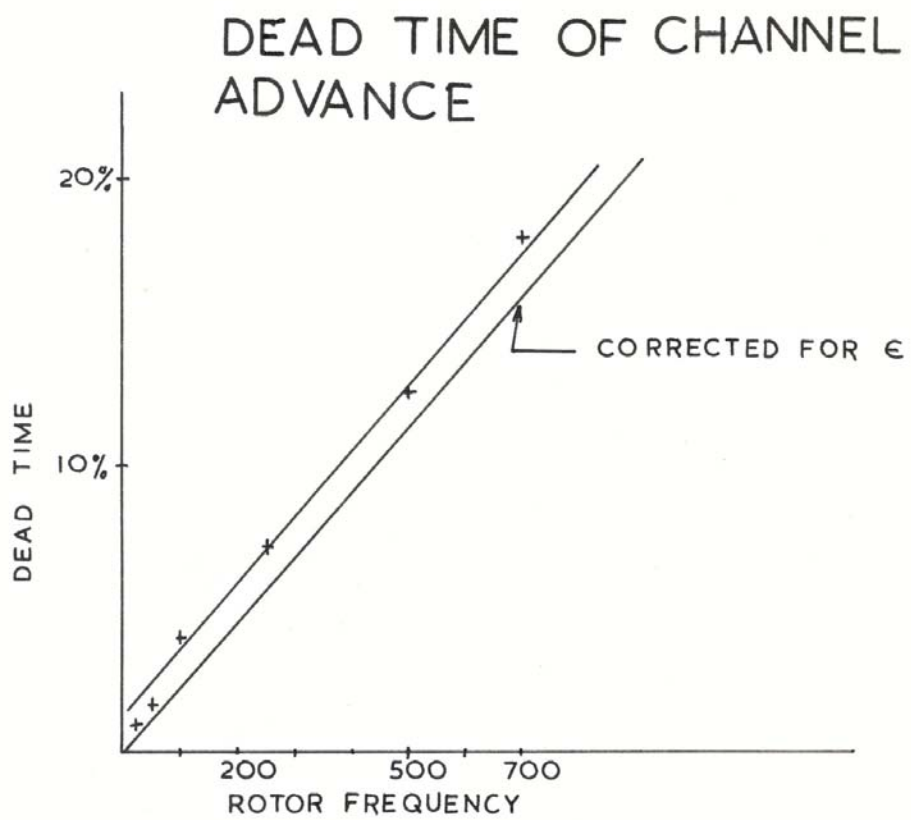

AT 700 CPS

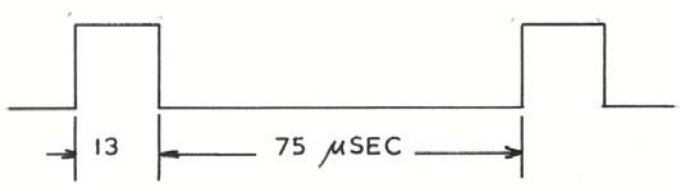

FIGURE 6.14

Using the strong ^{57}Co (Rh) source and a thin walled proportional counter the counting rates were in the region of 40,000 cts/sec subject to the decay of the source, the position of the rotor, and the window of the PHA. The investigation of the detector amplifier response indicates that there are no dead time effects up to a counting rate of 60,000 cts/sec. The PHA, with a response time of 1 μsec, will introduce a 4% dead time and the grand total scaler with a similar response time should not give rise to an additional dead time and can thus be taken to give a faithful account of the PHA output pulses.

The largest dead times will thus occur in the kicksorter as it takes 14 μsec to accumulate one pulse. Assuming then that this dead time is not extended, i.e. that pulses arriving during an accumulation cycle do not further extend the dead time, one can write the accumulation rate $\dot{n}$ as (Rainwater and Wu, 1947).

$$\dot{n} = \dot{N} / \left(1 + \dot{N}\tau\right) \qquad ...7.1$$

where τ is the time of accumulation and N the number of PHA pulses per second.

Hence
$$\frac{\dot{N}}{\dot{n}} \frac{d\dot{n}}{d\dot{N}} = 1 / \left(1 + \dot{N}\tau\right) \qquad ...7.2$$

which means that for $\dot{N}\tau << 1$ the slope is constant and the response to a change in the counting rate linear. For large counting rates the accumulation rate will asymptote to $1/\tau$ and the slope $\frac{\dot{N}}{\dot{n}} \frac{d\dot{n}}{d\dot{N}}$ will become zero. Considering this decrease in the slope with the statistical gain, which is proportional to $N^{1/2}$ one finds that the overall sensitivity is maximum for 35,000 cts/sec. This sensitivity S_1 is shown in Figure 6.15 and the arrow denotes the point of operation during the high speed run with the ^{57}Co (Rh) source.

To overcome this severe limitation a divider circuit can be incorporated between the PHA and the kicksorter, which would not only decrease the number of the pulses but also regularize their arrival. Using a by-m-divider network the probability for the occurrence of a pulse during a time interval dt and a time t after the arrival of a previous pulse is given by the Poisson distribution

$$P(t) = \frac{\dot{N}^m t^{m-1}}{(m-1)!} \; e^{-\dot{N}t}$$

from which the slope $\frac{\dot{N}}{\dot{n}} \frac{d\dot{n}}{d\dot{N}}$ and the resultant sensitivity can be calculated (Elmore, 1950) as shown in Figure 6.15 for m = 2, 4 and 16. The increase in the sensitivity is quite appreciable.

The choice of m is, however, limited by the rotor frequency. Taking $\dot{N}$ equal to 40,000 cts/sec and a rotor frequency of 700 cps, there will be on average 3.2 counts falling in each channel, which limits the scale of the dividing circuit to 4, if one does not want to average the angular dependent counting rate over more than 1.3 channels. Such a circuit has now been installed but new data are not yet available to be included in this thesis.

It would be possible to further increase the sensitivity if one could store the pulses occurring during the channel advance time. Such a logic circuit demanding the simultaneous presence of a pulse and the OPERATE level was considered. The increase in the sensitivity for m = 4 and 16 is also shown in Figure 6.15.

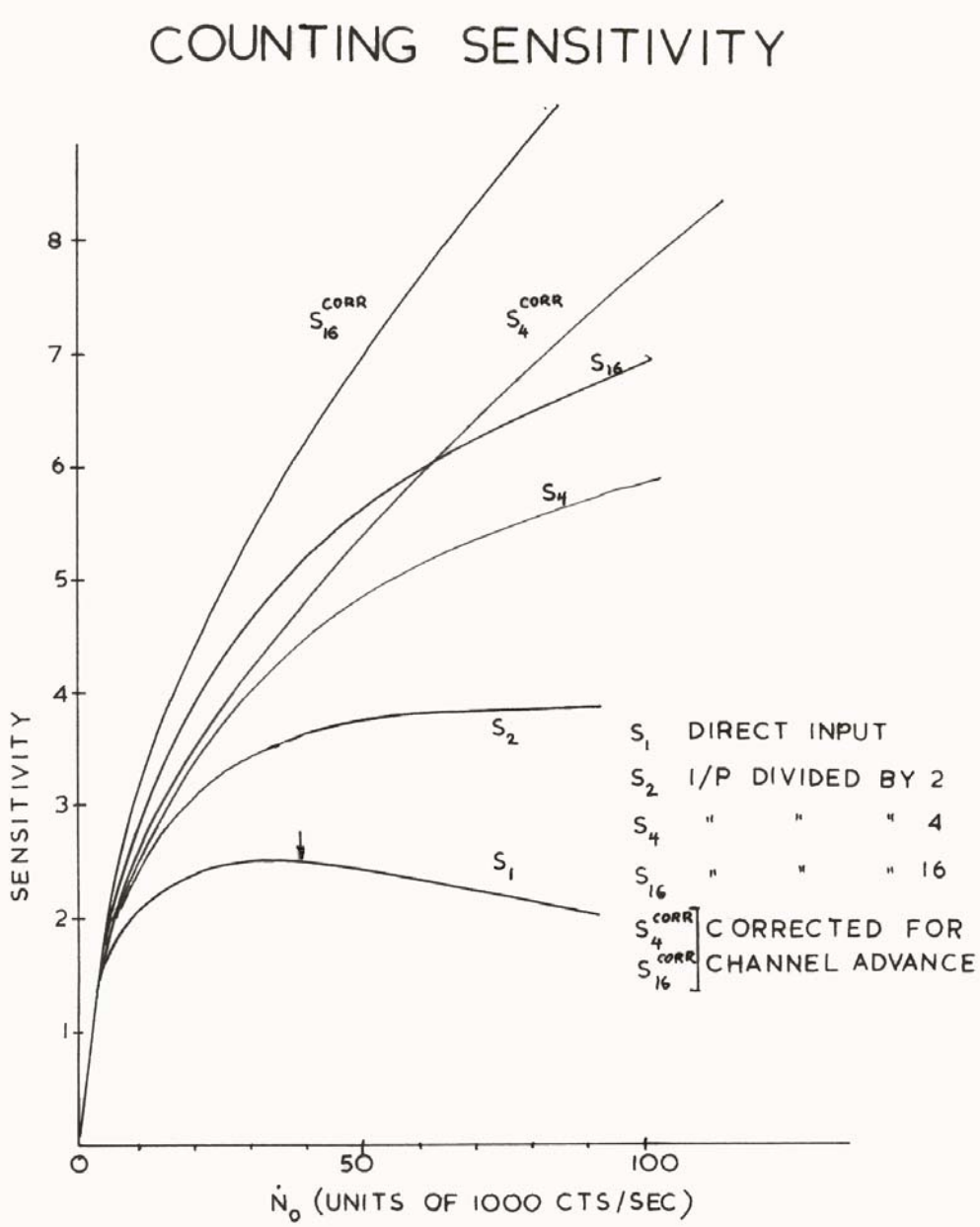
COUNTING SENSITIVITY
SENSITIVITY
8
7
6
5
4
3
2
1
0
50
100
$\dot{N}_0$ (UNITS OF 1000 CTS/SEC)
S_{16}^{CORR}
S_4^{CORR}
S_{16}
S_4
S_2
S_1
S_1 DIRECT INPUT
S_2 I/P DIVIDED BY 2
S_4 " " " 4
S_{16} " " " 16
S_4^{CORR}, S_{16}^{CORR} CORRECTED FOR CHANNEL ADVANCE

FIGURE 6.15

8. Alignment and Stability.

The aim of the experiment was to accurately monitor the angular and time dependent counting rate in $\dot{n}(0, t)$. To do this it was desirable to make all instrumental asymmetries as small as possible and ensure stable rotor running conditions. The instrumental effects, which could produce angular dependencies, consisted of the electronic asymmetry due to a non-equivalence of the 14 channels used, ii) the asymmetry of the detector response, and iii) the dependency of the counting rate on the rotor position.

Effect i) was found to produce an asymmetry of less than .05% and was thus negligible compared to the other two. Effect ii), upon rotation of the detector through 180°, produced a sinusoidal asymmetry of about 2.5%, which was probably the result of a misalignment between the axis of rotation of the detector and that of the rotor. The asymmetry also depended sensitively on the alignment of the tantalum collimator used to shield the lower portion of the counter. Once the detector had been positioned in the vacuum chamber, it was not possible to readjust it so that the position of the rotor was varied as a final parameter until the angular asymmetries in the counting rate were smaller than .2%. The adjustment was made at low rotor speed by moving the two adjustable damping assemblies.

As it was not thought that the angular dependent detector response would be as uniform as it turned out to be, provisions were made which allowed for a continuous rotation of the detector to average over the asymmetries. This meant rotating the whole table supporting the proportional counter, the EHT supply and the amplifiers.

Fortunately, this was not necessary, even though it was still desirable to rotate the detector at certain stages of the experiment to assess the effect of systematics on the error analysis of the data.

Once the system had been adjusted, it exhibited a remarkable long term stability. Figure 6.16 shows the total counts (~10^8) accumulated in each of the 14 channels during one day, i.e. 22 hours and 40 minutes of actual accumulation time, for 5 consecutive days. The asymmetry is .26% and is constant to within .02%. The 'short' term stability is shown in the second graph of Figure 6.16. It was obtained by dividing the day into four equal parts and displaying the counts accumulated in each during four consecutive days. This shows that the asymmetry is constant to within .015% which suggests that there were no observable diurnal variations in the counting rate.

During the experiment it was found, however, that the angular asymmetry was not constant for different rotor speeds (see Section 6.11). In order to find if this was a physical or an instrumental effect, attempts were made to monitor the rotor position. Such a measurement has to be sensitive to changes in the rotor position of .05 mm or less and it is not easy to obtain such an accuracy by conventional means. One system built consisted of an oscillator which measured the rotor position capacitatively. The frequency of the oscillator changed by ~1% for a 1 mm change in the rotor position, but the system was not very stable, the temperature coefficient being .02% per °C and the voltage coefficient .05% per 1% change in the supply voltage. As the oscillator was installed in the vacuum system, several other problems arose, caused by the mercury contacts used to connect the oscillator to the external power supplies and amplifier which made the measurement impracticable.

INSTRUMENTAL ASYMMETRIES

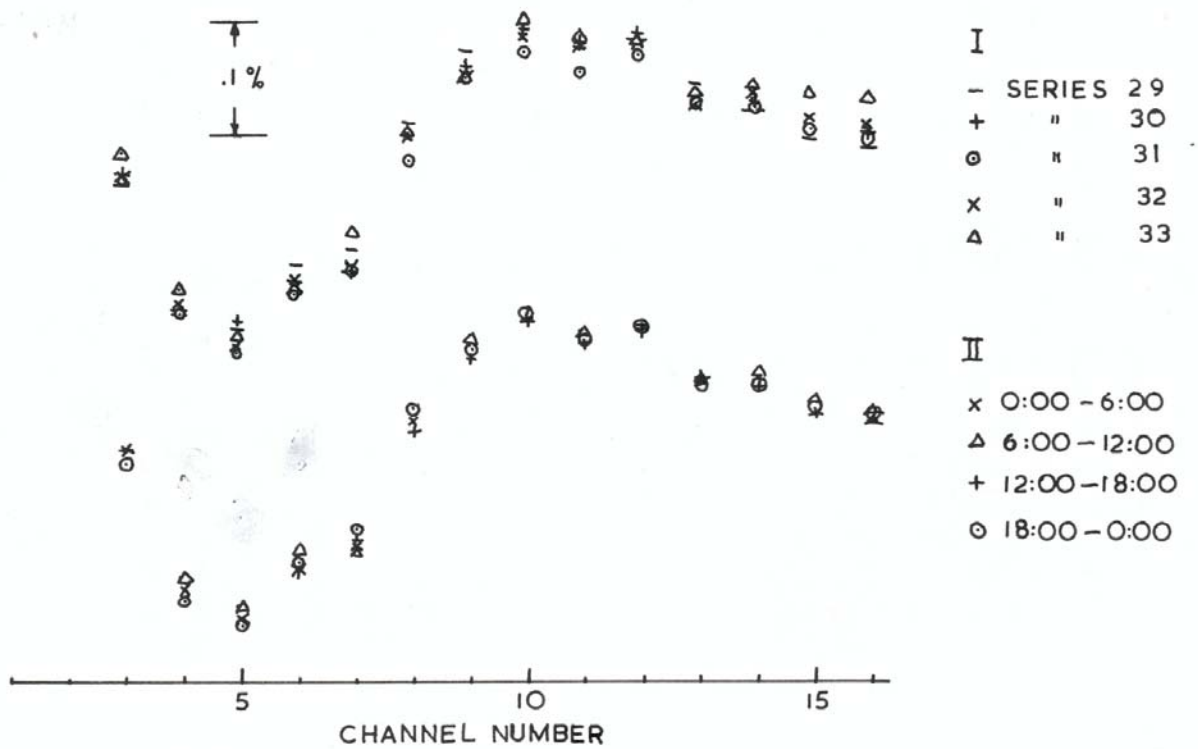

FIGURE 6.16

Another measuring device is presently installed, which detects a change in the core position to a potential accuracy of .01 mm, but as this does not measure the rotor position nor the imbalance of the rotor motion directly, the measurement is not very reliable.

9. Data Display.

Because of the high stability of the suspension system a simple program of data acquisition could be used. 16 runs each lasting 85 minutes were taken over a 24 hour period. The resulting 16 x 16 data points were arranged in a matrix and separately analyzed for each day. Because only 14 channels were used zeroes were substituted for the remaining two channels.

As one would classically expect a diurnally varying counting rate one can sum along the diagonals in the matrix (see Figure 6.17) so as to average out the instrumental asymmetries while superimposing the effects of an aether drift.

In order to give each row, i.e. each run, of the matrix equal weight the elements a_{ij} were multiplied by $16 \sum_{j=1}^{16} a_{ij} \Big/ \sum_{i,j=1}^{16} a_{ij}$. This correction amounted usually to less than .05%, determined mostly by the decay rate of the source of .257%/day.

The sums C_j of the elements along the 16 columns then give directly the instrumental asymmetries previously displayed in Figure 6.16. By summing the elements along the two diagonals one transforms the data into two frames of reference, one stationary in respect to the fixed stars and the other rotating at twice the angular velocity

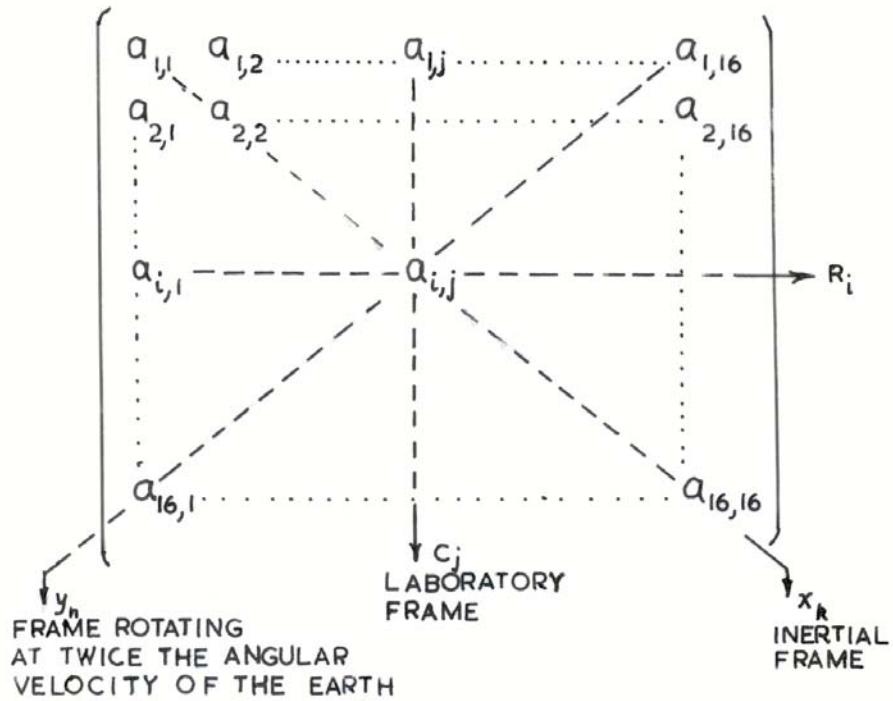
$a_{1,1}$ $a_{1,2}$ $a_{1,j}$ $a_{1,16}$
$a_{2,1}$ $a_{2,2}$ $a_{2,16}$
$a_{i,1}$ $a_{i,j}$ R_i
$a_{16,1}$ $a_{16,16}$
C_j
LABORATORY FRAME
y_n
FRAME ROTATING AT TWICE THE ANGULAR VELOCITY OF THE EARTH
x_k
INERTIAL FRAME

FIGURE 6.17

of the earth, the sums for the respective frames denoted by x_k and y_n. Fitting these values to a sine-function one can analyze their statistical behavior knowing that only the x_k values would exhibit aether drift effects, while both would be equally affected by systematics.

A computer was used to calculate

$$X^m(A,\mathrm{j}\ ) = \frac{1}{15}\sum_{k=1}^{16}\left(x_k - \mathrm{A}\sin\left(\frac{2\pi k}{16} + \mathrm{j}\ \right)\right)^2 \qquad ...9.1.$$

$$Y^m(B,\delta) = \frac{1}{15}\sum_{n=1}^{16}\left(y_n - \mathrm{B}\sin\left(\frac{2\pi n}{16} + \delta\right)\right)^2 \qquad ...9.2.$$

for the m different run series, where A and B were varied in 16 incremental steps to a maximum value of about 3 x 10^{-4} x_k depending on the total counts accumulated. Similarly the phases of j and δ were varied in 16 steps making up 2π. From the resulting 16 x 16 array the values A_0, j_0 and B_0, δ_0 could be found, which minimized X^m (A, j) and Y^m(B, δ). The associated errors could also be readily found after applying a dead time correction.

10. Running Time.

In total 40 run series each lasting 24 hours were taken. The run series were well spread over the whole year with five major ones taken in July, August, October, April and May. Table 6.5 shows the number of run series taken with the corresponding source-absorber combinations. The slopes shown are deduced from the actual changes in the counting rate observed during the rotor runs.

Table 6.5.

Number of run series	Number of runs	Rotor frequency	Source	Absorber	Slope $\left(\frac{n}{N}\frac{dN}{dn}\right)$
3	66	60	10 mCi ^{57}Co(Pd)	S.F.C. (T_a□ 8)	1.22 x 10^{11}
2	35	200			1.35 x 10^{11}
19	328	425			1.15 x 10^{11}
2	33	250	40mCi ^{57}Co(Rh)	S.F.C. (T_a□ 4)	1.16 x 10^{11}
1	16	495			0
1	16	676			1.30 x 10^{11}
1	19	250	40mCi ^{57}Co(Rh)	S.F.C. (Ta□ 8)	1.96 x 10^{11}
2	34	650			1.75 x 10^{11}
9	151	701			2.18 x 10^{11}

11. Data Analysis.

Assuming the presence of an aether drift in westerly direction and a clockwise rotor motion, the energy of the source when pointing North, as seen by the absorber, will be increased. This would produce a decrease in the counting rate when operating at the lower point of inflection and an increase at the higher point of inflection. One then obtains the following normalized angular dependent counting rates (see Section 4.3).

$$\dot{n}(\theta) \quad = 1 + \frac{UV}{c^2}\left(1 + \delta\left(\frac{V}{c}\right)\right)\sin\theta \qquad \text{...11.1 a}$$

$$= 1 + \frac{A_\circ^{\,m}}{R^m}\left(\frac{\mathrm{N}}{\mathrm{n}}\ \frac{\mathrm{dn}}{\mathrm{dN}}\right)\left(\frac{\dot{n}}{\dot{N}}\ \frac{d\dot{N}}{d\dot{n}}\right)\sin \mathrm{j} \qquad \text{...11.1 b}$$

where $\frac{\mathrm{n}}{\mathrm{N}}\ \frac{\mathrm{dN}}{\mathrm{dn}}$ is the slope of the resonance at the operating rotor velocity and R^m is the corrected sum of the row elements for run series m. The factor $\frac{\dot{n}}{\dot{N}}\ \frac{d\dot{N}}{d\dot{n}}$ corrects for the decrease in the counting rate response of the kicksorter and amounts to $\left(1 + \dot{N}\tau\right)$.

The aether drift is then simply to first order

$$V^m = \frac{A_\circ^{\,m}}{R^m}\left(\frac{N}{\mathrm{n}}\ \frac{d\mathrm{n}}{dN}\right)\left(1 + \dot{N}\tau\right)\frac{c^2}{U} \qquad \text{...11.2.}$$

The parameters that can be extracted from the data are V^m and $j_\circ^{\,m}$ the phase angle between $\underline{V}$ and $\underline{V}^m$, and analogously I^m and $\delta_\circ^{\,m}$ which are the instrumental effects as deduced from equation 6.11.2 by substituting B_0^m for A_0^m. By comparing V^m with I^m one can differentiate between real and instrumental effects and determine the statistical significance of any fluctuations observed.

Even though a total of 40 run series were taken, only those results will be discussed that were obtained with the ^{57}Co(Rh) source as the accuracy of one run series taken with the stronger source was comparable with the combined result of all the runs taken with the weaker source. The latter result was V<(2.1±16) cm/sec and is displayed with the more accurate data. In table 6.6 the result of the 11 high speed run series is shown. The asterisk denotes the run that was taken with the thin absorber (T_a □ 4).

Table 6.6

Run series	Rotor frequency	V^m(cm/sec)	$j_\circ^m$ (0°=N)	I^m(cm/sec)	$\delta_\circ^m$ (0°=N)
25	678	19.0	350	9.8	230
27	650	5.6	250	13.6	350
28	650	9.3	45	9.85	180
29	701	7.75	155	3.4	225
30	701	9.75	190	8.75	45
31	701	16.2	30	3.0	215
32	701	5.45	20	2.0	190
33	701	15.5	315	3.6	270
35	701	3.4	250	5.0	340
36	701	9.35	190	3.0	0
37	701	6.95	215	7.15	90
		V^m_{AVE} = 9.82 cm/sec		I^m_{AVE} = 6.28 cm/sec	

Table 6.7

Run Series m	Rotor Speed CPS	R^m $x10^{-6}$	R^m_c $x10^{-6}$	$X^m(0)$ $x10^{-6}$	$Y^m(0)$ $x10^{-6}$	$X^m(A_0)$ $x10^{-6}$	$Y^m(B_0)$ $x10^{-6}$	$X^2_{15}(X)$	$X^2_{15}(Y)$	$X^2_{13}(X)$	$X^2_{13}(Y)$
22+	250	94.68	42.9	56.6	40.0	21.0	25.8	19.8	14.0	7.4	9.1
23+	250	92.46	41.8	221.8	173.5	187.2	140.8	79.5	62.0	66.8	50.5
26	250	82.43	42.8	165.4	99.0	51.0	35.0	59.4	35.5	18.3	12.5
AVE.:		89.86	42.5	148.0	104.2	86.4	67.2	52.9	37.1	30.8	24.0
24+	495	84.21	39.2	63.8	106.4	40.2	67.8	24.4	33.9	15.4	25.9
34	701	87.28	36.7	197.5	165.7	24.1	35.5	82.0	68.5	10.0	14.7
25+	678	79.60	36.3	25.0	23.6	10.6	19.7	10.4	9.8	4.4	8.2
27	650	87.69	37.2	17.4	43.3	15.0	29.4	7.0	17.5	6.1	11.9
28	650	87.76	37.3	39.4	32.3	32.9	25.0	15.9	13.0	13.2	10.0
29	701	87.40	36.1	23.3	28.4	15.2	27.0	9.6	11.8	6.3	11.2
30	701	87.44	36.1	39.7	46.5	26.9	36.3	16.4	19.3	11.1	15.0
31	701	87.39	36.4	82.9	24.7	47.2	23.8	34.3	10.3	19.5	9.9
32	701	87.31	36.5	42.1	30.1	37.8	29.5	17.5	12.5	15.7	12.2
33	701	87.28	36.5	55.6	25.0	23.3	23.3	23.0	10.4	9.7	9.7
35	701	87.64	36.8	27.8	39.3	26.4	36.1	11.5	16.2	10.9	14.9
36	701	86.78	36.7	60.7	40.6	48.8	39.5	25.1	16.8	20.1	16.3
37	701	87.18	36.8	32.1	41.3	25.7	34.3	13.2	16.9	10.5	14.1
AVE.:		86.72	36.6	40.5	34.1	28.1	29.4	16.4	13.7	11.4	11.8

Averaging the magnitudes of V^m and I^m one finds that the former exhibit a larger fluctuation than those values representing the pure instrumental effects. This is further brought out by displaying the results in polar diagrams. Figure 6.18 shows the V^m values relative to north, the direction in which one would classically expect a larger counting rate. Several runs do indeed show a larger fluctuation in that direction unlike the results of I^m shown in Figure 6.19 which are more evenly weighted in all directions. In the error analysis given below one finds however, that the results are well within statistics and that the experiment is not sensitive enough to distinguish between real and instrumental effects. Adding vectorially the results for the 11 run series at high speed and the 19 at low speed one obtains $V<(2.0 \pm 5.2)$ cm/sec compared to $I<(0.7 \pm 5.2)$ cm/sec.

The real difficulty in the analysis arises when trying to assess the statistical and systematical errors. To do this accurately one would have to know the exact behavior of the kicksorter under high counting rates. In the above analysis it was assumed that the kicksorter (type RCL) has a non-extended dead time and no buffer storage. While the first assumption is realistic the second assumption could not be verified without fully understanding the logic circuitry used in the kicksorter. Empirically it was found that the counts accumulated in the kicksorter did approximately follow the dependence expressed by equation 6.7.1, which substantiated the two assumptions made.

In that case one can calculate the expected variance under high counting rates (Feller, 1948) given by

$$\sigma^2 = \frac{n}{\left(1+\dot{N}\tau\right)^2} \qquad \text{...11.3.}$$

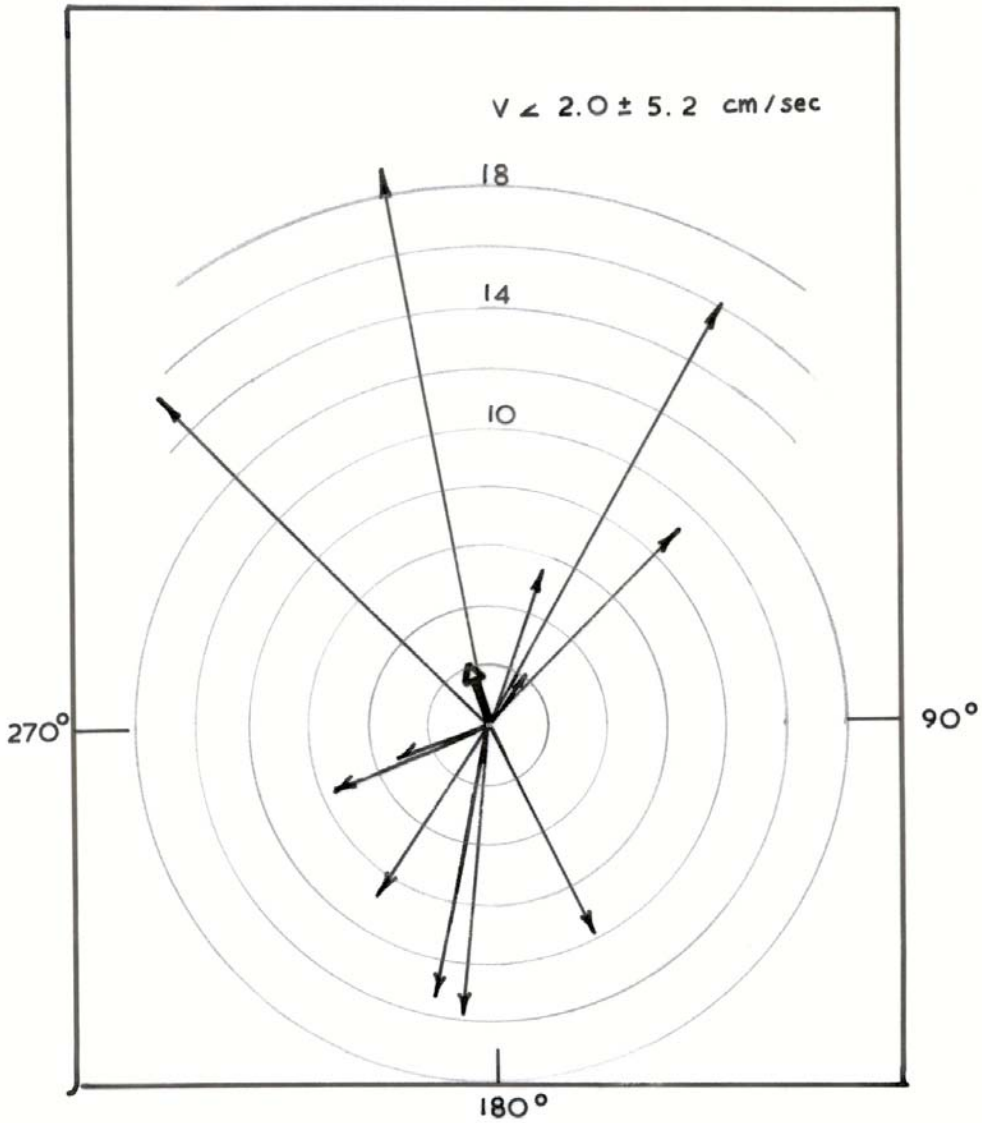

FIGURE 6.18

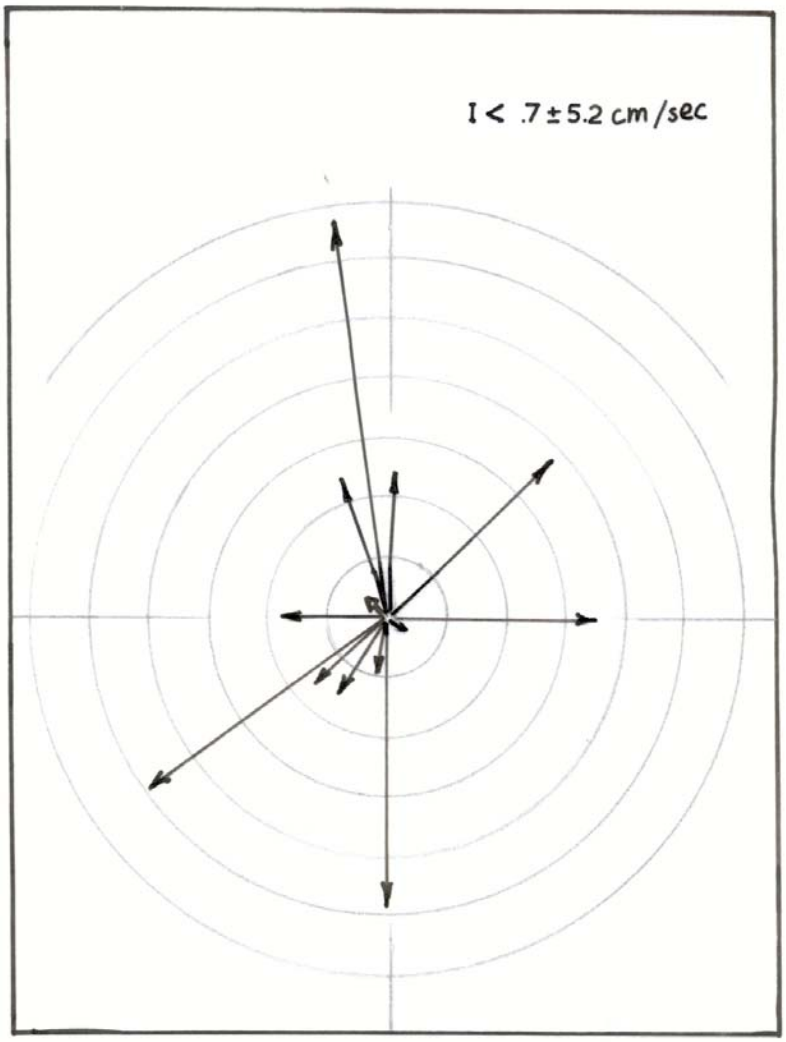

FIGURE 6.19

Where σ is the standard deviation of n counts accumulated. Table 6.7 gives, for the individual run series, the average of the total counts accumulated in the 16 effective channels x_k and y_n (equal to R^m) and the expected variance $R^m/(1+\dot{N}\tau)^2$ denoted by $R_c^{\ m}$. The actually determined sample deviations

$$X^m(0) = \frac{1}{15}\sum_{k=1}^{16}(x_k - \overline{x})^2 \qquad \text{...11.3a}$$

$$Y^m(0) = \frac{1}{15}\sum_{n=1}^{16}(y_n - \overline{y})^2 \qquad \text{...11.3b}$$

can then be directly compared with the expected variance to determine the consistency of the results. $X^m(0)$ and $Y^m(0)$ are also shown in table 6.7, as well as the fitted values $X^m(A_o, j_o)$ and $Y^m(B_o, \delta_o)$. Considering the run series taken at high speed (m = 25, 27-33, 35-37), one finds that the sample deviations agree well with the expected variances with a suggestion that the $X^m(0)$ values are larger than the $Y^m(0)$ values. To analyze these figures more quantitatively the values of X^2 have been calculated, where

$$X_{15}^2\left(X^m(0)\right) = \frac{\sum_{k=1}^{16}\left(x_k - \overline{x}\right)^2}{R_c^{\ m}} = \frac{15X^m(0)}{R^m_{\ c}} \qquad \text{...11.4a}$$

$$X_{15}^2\left(Y^m(0)\right) = \frac{15Y^m(0)}{R^m_{\ c}} \qquad \text{...11.4b}$$

$$X_{13}^2\left(X^m(A_\circ, j_\circ)\right) = \frac{15X^m(A_\circ, j_\circ)}{R^m_{\ c}} \qquad 11.4c$$

$$X_{13}^2\left(Y^m(B_\circ, \delta_\circ)\right) = \frac{15Y^m(B_\circ, \delta_\circ)}{R^m_{\ c}} \qquad 11.4d$$

The subscripts of X^2 denote the number of degrees of freedom of the respective experimental values.

The expected values are $X_{15}^2 = 14.3_{-4.5}^{+5.9}$ and $X_{13}^2 = 12.3_{-4.1}^{+5.4}$. Considering again the high speed run series (m = 25, 27-33 and 35-37), one finds that the average values of equation 6.11 fall well within the expected X^2 intervals, but that $X^2(X^m(0))_{AVE}$ is somewhat larger than $X^2(Y^m(0))_{AVE}$. This fact is further brought out by considering the individual values. Whereas all the values of $X_{15}^2\left(Y^m(0)\right)$ and $X_{13}^2\left(Y^m(B_\circ,\delta_\circ)\right)$ fall within the expected interval, five values of each $X_{15}^2\left(X^m(0)\right)$ and $X_{13}^2\left(X^m(A_\circ,\mathrm{j}_\circ)\right)$ fall outside the interval indicating that the X^m values have a significantly higher fluctuation, i.e. those terms that are sensitive to aether drift effects show a larger deviation.

One might argue, however, that in an experiment of the present type, where one compares the data taken over a 24 hour period, one would inevitably expect some excess fluctuations to occur. In fact the results are so consistent with X^2 and some values even smaller than expected, that one might be skeptical if there isn't some additional smoothing effect that averages the data during accumulation. Such an effect cannot be ruled out on our present knowledge of the operation of the kicksorter. Certainly if the fluctuations are as low as indicated above then the method of analysis used here is well justified and added confidence is given to the results.

That the analysis does indeed show up instrumental effects is brought out by run series 34 where a deliberate asymmetry of 2.5% was introduced by rotating the proportional counter. The values of $X_{15}^2\left(X^{34}(0)\right)$ and $X_{15}^2\left(Y^{34}(0)\right)$ fall well outside the interval, whereas

the fitted values do agree satisfactorily suggesting that the asymmetry could be well represented by a sine-function.

The results of the other runs (m = 22, 23, 26) further show that the analysis is affected by instrumental effects. During those runs the +12 volt supply line was observed to fluctuate by .2 volt causing a .6% change in the counting rate, and also during these short run series the system did not have time to come to an equilibrium. These factors are brought out by the excess fluctuations observed for these run series.

Table 6.8

Run Series	V^m(cm/sec)	$j_\circ^m$ (0° = North)	I^m(cm/sec)	$\delta_\circ^m$ (0° = North)
25+	19.0 ± 30.1	350 ± 110	9.8 ± 30.3	230 ± large
27	5.6 ± 22.1	250 ± large	13.6 ± 22.6	350 ± 110
28	9.3 ± 21.5	54 ± large	9.85 ± 21.5	180 ± large
29	7.75 ± 15.9	155 ± large	3.4 ± 16.3	225 ± large
30	9.75 ± 16.3	190 ± 110	8.75 ± 16.3	45 ± 170
31	16.2 ± 16.2	30 ± 60	3.0 ± 16.2	215 ± large
32	5.45 ± 16.7	20 ± large	2.0 ± 16.5	190 ± large
33	15.5 ± 16.3	315 ± 60	3.6 ± 16.5	270 ± large
35	3.4 ± 16.5	250 ± large	5.0 ± 16.5	340 ± large
36	9.35 ± 16.5	190 ± 120	3.0 ± 16.5	0 ± large
37	6.95 ± 16.5	215 ± large	7.15 ± 16.5	90 ± large
8-21	2.1 ± 16.0	340 ± large	.5 ± 16.0	120 ± large

In order to determine the errors associated with the values of V^m, $j_\circ^m$ and I^m, $\delta_\circ^m$ quoted previously, the 16 x 16 arrays of $X^m(A, j)$ and $Y^m(B, \delta)$ were analyzed to find those values of A_1 and B_1 that would increase $X^m(A_o, j_\circ)$ and $Y^m(B_o, \delta_\circ)$ by R^m_c, i.e. by one standard deviation. The errors for the two phases $j_\circ^m$ and $\delta_\circ^m$ were found similarly, however, for some of the run series the dependence of phase was not very strong so that no definite error could be assigned to them. The final values and associated errors are shown in the table 6.8.

As discussed before, the values for V^m fall within statistics. The limit set by the present experiment on effects arising from the translational motion of the earth is (2.0 ± 5.2) cm/sec with $j_\circ$ = 340° ± large.

In the above analysis only that component of V arising from the translational velocity of the earth has been considered. To put a limit on effects arising from the rotation of the earth, which would appear as a time independent asymmetry in $\dot{n}(0)$ at a given rotor speed, one would have to analyze $\dot{n}(0)$ for two different velocities, preferably at points located at opposite sides of the resonance curve. This was done for rotor frequencies of 250, 495 and 676 cps. The angular asymmetries measured at these speeds are shown in Figure 6.20. As the experiment is insensitive to the aether drift at 495 cps, one can determine the net changes in the asymmetry for the run series taken at 250 cps and 676 cps, which are shown in Figure 6.21. The results indicate that $\dot{n}(0)$ has changed appreciably even though none of the other experimental parameters has been altered. The 'aether drift' deduced from the high

speed run is 3.6 m/sec. As, however, the asymmetry observed for the low speed run is comparable with

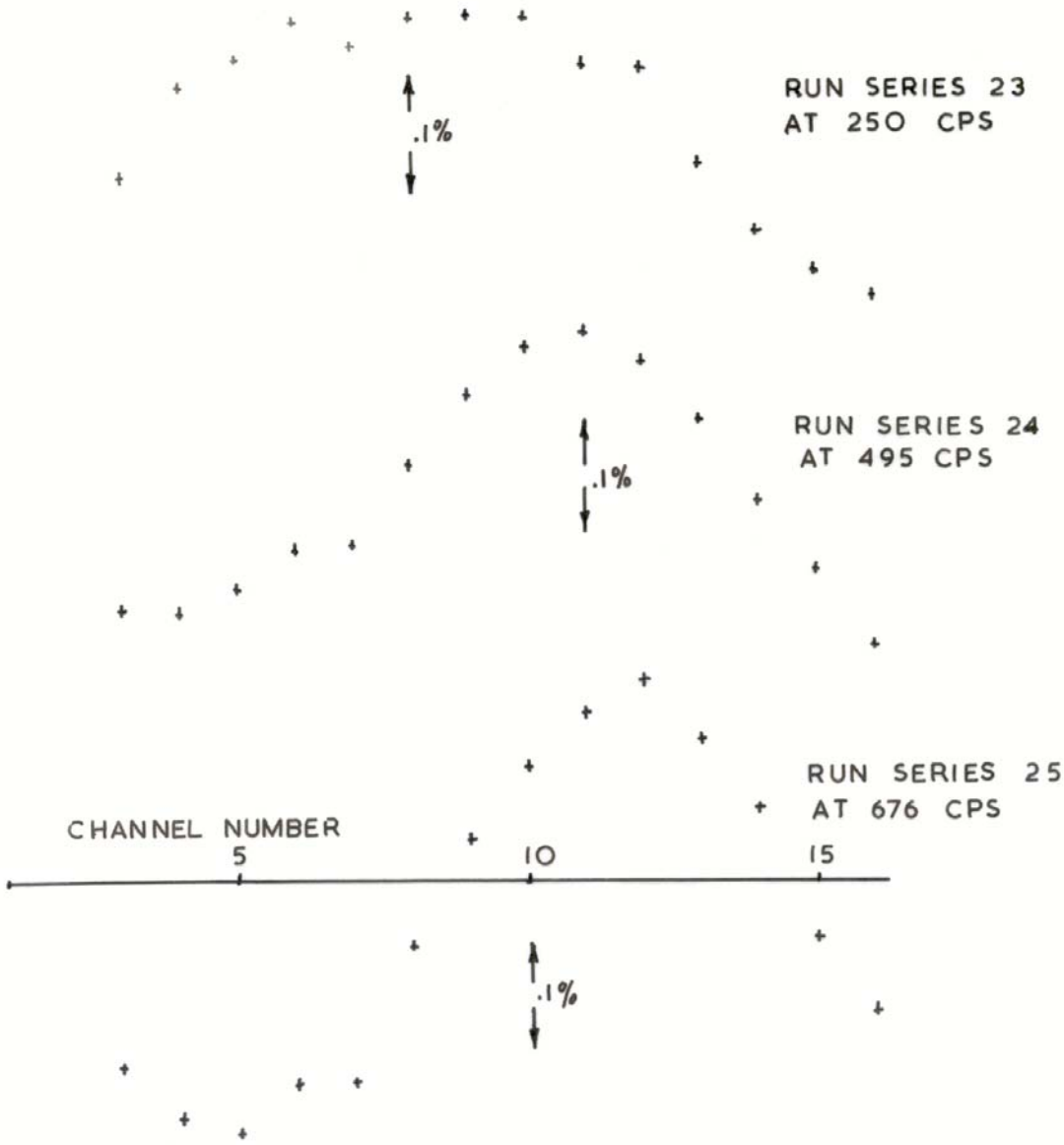
RUN SERIES 23
AT 250 CPS
.1%
RUN SERIES 24
AT 495 CPS
.1%
RUN SERIES 25
AT 676 CPS
CHANNEL NUMBER
5
10
15
.1%

FIGURE 6.20

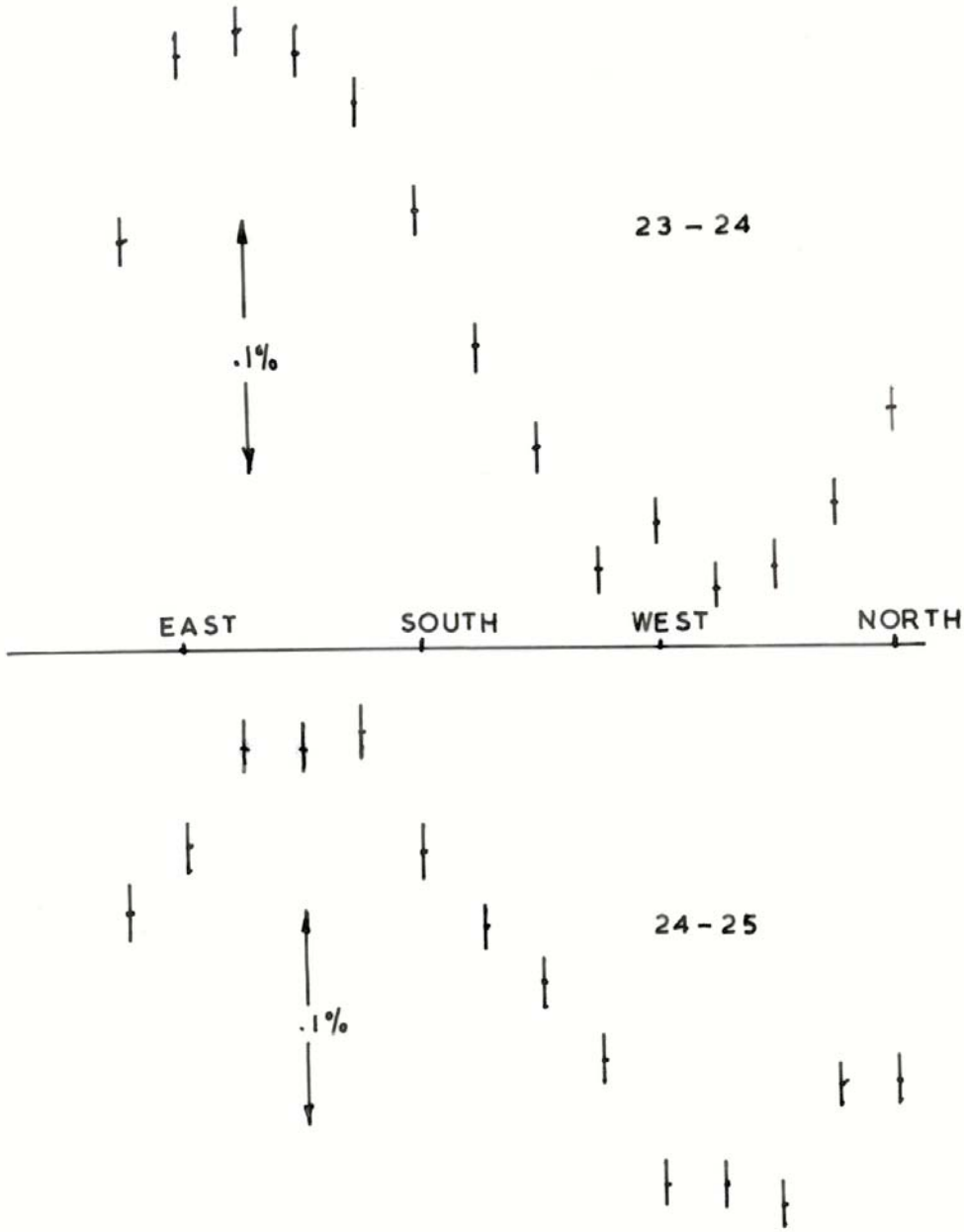

FIGURE 6.21

that at 676 cps and not smaller, as one would expect because of the lower sensitivity at low speeds one can conclude that the observed asymmetry is caused by instrumental effects. To establish this more conclusively, one has to monitor the position of the rotor as a function of its velocity. The difficulties inherent in such a measurement have been discussed previously, but nevertheless a system is presently installed to measure the position of the core from which the time averaged position of the rotor can be deduced.

12. Future Improvements.

In order to investigate some of the problems discussed in this chapter, it is planned to have another series of runs lasting several weeks. Even though the source has decayed since the last run series by .7 of one half life, it should still be possible, with a number of improvements, to achieve a higher sensitivity than before. Assuming that the efficiency of the present counter has not changed, so that, with the present source, one would obtain a counting rate of 25,000 cts/sec, the sensitivity would be increased by a factor of 1.7 by introducing the by-4 divider network between the PHA and the kicksorter. Furthermore, more uniform S.F.C. absorber would increase the sensitivity by another factor of 1.4, which would give an overall increase of 2.4. This should be a sufficient increase to investigate in more detail the fluctuations observed at high speed, and would also reduce the limit to the 2 cm/sec level.

The ultimate sensitivity of the experiment is limited by the saturation effects observed with the present counting electronics and the maximum tip speed of the rotor. Assuming one could get a ~60 mCi source one would obtain the optimum counting rate, which would improve the sensitivity by a factor of 2.6.

As shown in figure 5.8 the top part of the rotor is designed for a tip velocity of 700 m/sec, which is more than twice the velocity used in the experiment. As the maximum speed does, however, depend on the strength of the rim and the bond between the rotor and the absorber skirt, both of which cannot be directly calculated, it is questionable if the speed can be much increased. The practical limit is 950 cps for a copper source and a chromium absorber, which would increase the sensitivity by 1.35 and the total sensitivity using maximum counting rates by about 5 over that achieved with the present experiment. This, however, would only improve upon the result obtainable with the present source by a factor of 2 which does not really warrant the expense of a new source. It appears thus that the experiment has reasonably well exhausted the potential accuracy of the equipment.

13. Discussion.

Figure 6.22 shows the result of the present experiment in relation to the ones previously conducted. The limit set on the existence of a preferred frame of reference is about six orders of magnitude smaller than that due to the motion of the earth around the sun.

In the spirit of the analysis given by Robertson, one would distinguish between the two frames of reference X and X^1, one at rest and the other in motion relative to the 'fixed stars.' In a four dimensional Euclidian space the four coordinates are then related by

$$ds^2 = dx^2 + dy^2 + ds^2 - c^2 dt^2$$

where rods and clocks are used to measure space-like and time-like intervals. In the second coordinate frame moving along the x-axis with velocity v relative to the rest frame

$$ds^2 = g_1{}^2 dx'^2 + g_2{}^2 \left(dy'^2 + dz'^2 \right) - g_\circ{}^2 c^2 dt'^2$$

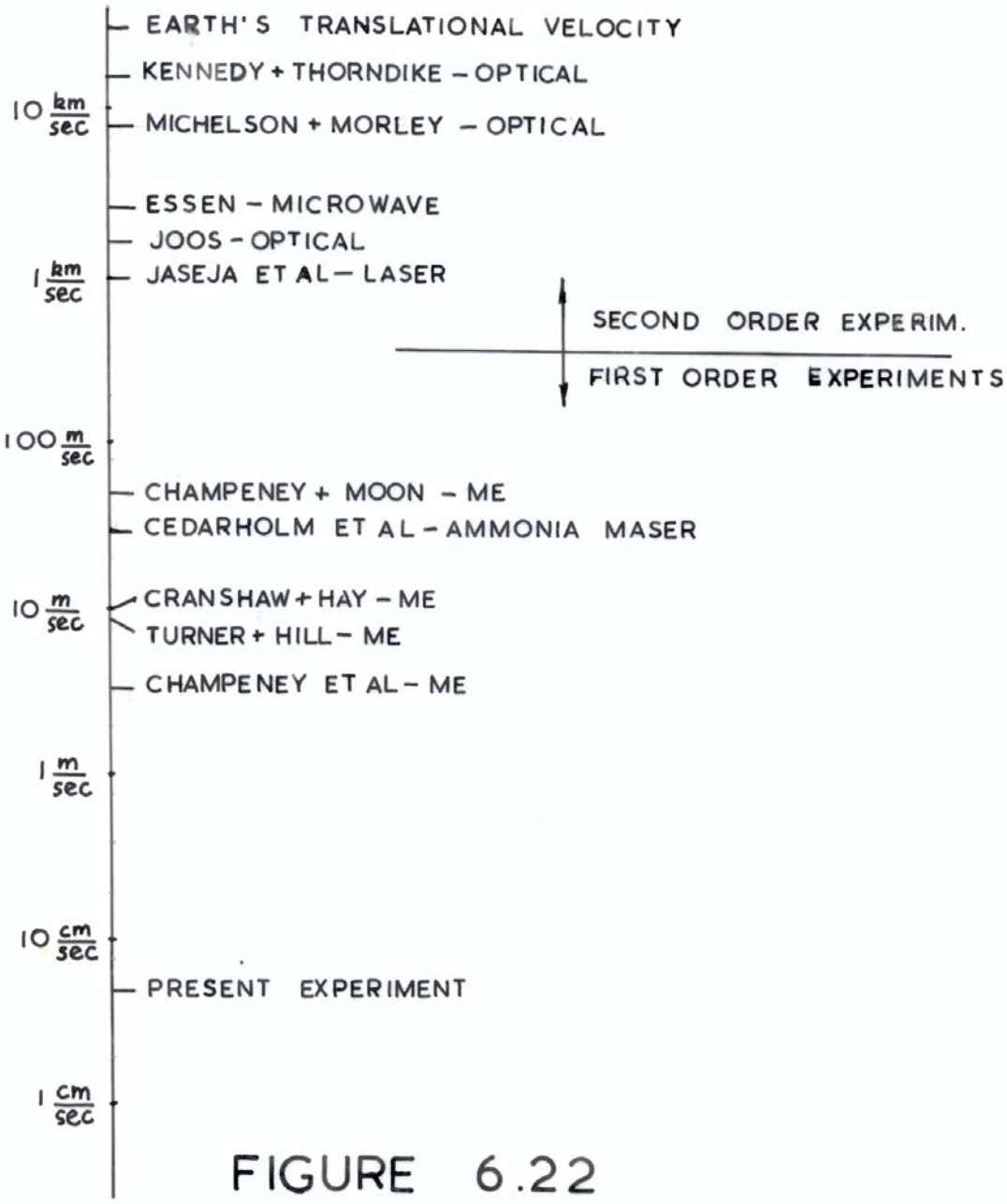
EARTH'S TRANSLATIONAL VELOCITY
KENNEDY + THORNDIKE – OPTICAL
10 km/sec
MICHELSON + MORLEY – OPTICAL
ESSEN – MICROWAVE
JOOS – OPTICAL
1 km/sec
JASEJA ET AL – LASER
SECOND ORDER EXPERIM.
FIRST ORDER EXPERIMENTS
100 m/sec
CHAMPENEY + MOON – ME
CEDARHOLM ET AL – AMMONIA MASER
10 m/sec
CRANSHAW + HAY – ME
TURNER + HILL – ME
CHAMPENEY ET AL – ME
1 m/sec
10 cm/sec
PRESENT EXPERIMENT
1 cm/sec

FIGURE 6.22

where the coordinates are measured in the moving frame and are given by the Lorentz transformation expressed by equation 4.2.1. The quantities g_0, g_1, g_2 are given by

$$g_\circ = a_\circ^{\circ/\gamma} \qquad a_\circ^\circ / \gamma$$

$$g_1 = a_1^{1/\gamma} \qquad a_1^1 / \gamma$$

$$g_2 = a^2{}_2 \qquad a_2^2$$

where $a_1{}^1$ is the transformation coefficient between dx and dx^1, $a_2{}^2$ that between the other spacial coordinates and $a_0{}^0$ that between dt and dt^1. Because of the Lorents invariance of ds^2 the special theory of relativity fully determines the three quantities $g_1 = g_2 = g_0 = 1$. In general to check the equivalence between the two frames of reference X and X^1, one would have to experimentally determine the set of three quantities.

According to Robertson the experiments of Michelson and Morley, Kennedy and Thorndike, and Ives and Stilwell measure the respective quantities g_1/g_2, g_0/g_1, and g_0 and so fully determine the transformation properties between frames X and X^1. Accurate measurements of these quantities then would not only serve as a test of the fundamental postulates of the special theory and the Lorentz transformation but also as a sensitive method to detect any anisotropies in the propagation of light.

Taking the translational velocity of the earth around the sun as the relevant velocity parameter, the above experiments establish the g- coefficients to the following accuracies:

i) the most accurate optical experiment by Joos (1938) established g_1/g_2 to within 1 part in 400,

ii) the Kennedy and Thorndike experiment determines g_0/g_1 to within 1 part in 4 and the experiment by Jaseja et al. (1964) improves this to 1 part in 10^3,

iii) the result obtained by Mandelberg and Witten establishes g_0 to within 1 part in 20, and the more accurate experiments conducted using the Mössbauer effect improve this result by a factor of 4.5.

Considering the present experiment in this context, one finds that it is sensitive to both g_0 and g_0/g_1 (see section 4.3). It establishes g_0 to within 3 parts in 10^{12}. As the experiment is sensitive to the second order terms (in equation 4.3.6), which are affected by the Lorentz-Fitzgerald contraction, it determines g_0/g_1 to an accuracy of 3 parts in 10^4.

In the above analysis the earth's translational velocity was taken as the relevant parameter. In order to establish the true local rest frame in the cosmological sense one would not only have to know the mass-velocity distribution of the universe but also the detailed interaction between local and distant matter. One approach to the latter problem is given by the theory of inertia as developed by Sciama (1953). According to this theory the contribution of matter to local inertia falls off with the inverse of the distance, so that the relative contributions of the earth, sun, and our galaxy to local inertia are 10^{-9}, 10^{-8} and 10^{-7} respectively, i.e. are negligible compared to the contribution of the universe as a whole. Thus, if one takes the inertial forces as a criterion for determining the local rest frame one might well find that the relevant velocities for the aether drift experiment are much larger than those considered here, as they would be determined by the velocity distribution of distant matter, which could be large indeed. In this context the present experimental results would then establish the principle of relativity to an even higher accuracy.

14. Emission Theories of Light Propagation.

It has recently been suggested (Fox, 1962, 1965) that the emission theories of light, which stand in contradiction to the special theory of relativity, have not been as thoroughly disproven as had generally been thought. As in these theories light is considered to be emitted with velocity c relative to the source, the outcome of the present experiment would become self evident. Hence it is desirable at this point to briefly review the main experiments conducted recently, that have now provided the evidence against such theories.

Before 1962 the main evidence came from the observation of binary stars, but as Fox pointed out this evidence was not conclusive as the effect of the extinction and reemission of light in interstellar matter had not been considered. According to Ewald and Oseen, primary radiation (of wavelength λ) when entering a medium with index of refraction n, is extinguished in a distance $d = \lambda/2\pi(n-1)$ and is replaced by secondary radiation (of same frequency but different propagating velocity), which is emitted by the forced oscillations of the radiating dipoles in the medium.

Experiments designed to test the emission hypothesis must thus be entirely free of extinction effects in order to give a conclusive result. Kantor (1962), who performed the first optical experiment in which this condition was met, did obtain a result consistent with the emission hypothesis, but later more carefully conducted experiments (Babcock and Bergman, 1964; Beckman and Mandice, 1964) did give results consistent with the special theory of relativity.

The more convincing experiments are those conducted with high energy gamma rays, even though they are subject to some extinction effects in the target material. The most

accurate experiment and one in which the extinction length between source and absorber was the smallest so far reported, less than .03 d, was performed by Alvager et al. (1964), who measured the time of flight of gamma rays produced by the decay of 6 GeV π° mesons and found it to be consistent with c to an accuracy of 2 parts in 10^4.

This result was also verified by the present author, in an experiment suggested by A.M. Khan, by using the ^{57}Co(Rh) source and a stainless steel absorber. The geometry of the experiment was as shown in Figure 6.23, where the source was mounted on a motion device outside of the vacuum chamber and a Mylar window allowed the radiation to penetrate through the chamber walls. The radiation passing through the collimators was dragged by the beryllium skirt of the rotor, which was spinning at approximately 10 cps. If the propagating velocity of the 14.4 kev radiation had been modified by the motion of the beryllium skirt, which had an extinction length of about 1.5 x 10^3d, then the resonance dip with the .0001" thick stainless steel absorber (with an extinction length smaller than. 3d) should have been markedly decreased. Instead the R_m observed with the spinning rotor was consistent to better than 3.5% with the R_m determined for the case of no rotor which is in satisfactory agreement with expectations.

These experiments do indicate that the propagation of light is unaffected by the motion of the source and in conjunction with the aether drift experiment represents a most accurate verification of the fundamental postulates of the special theory of relativity.

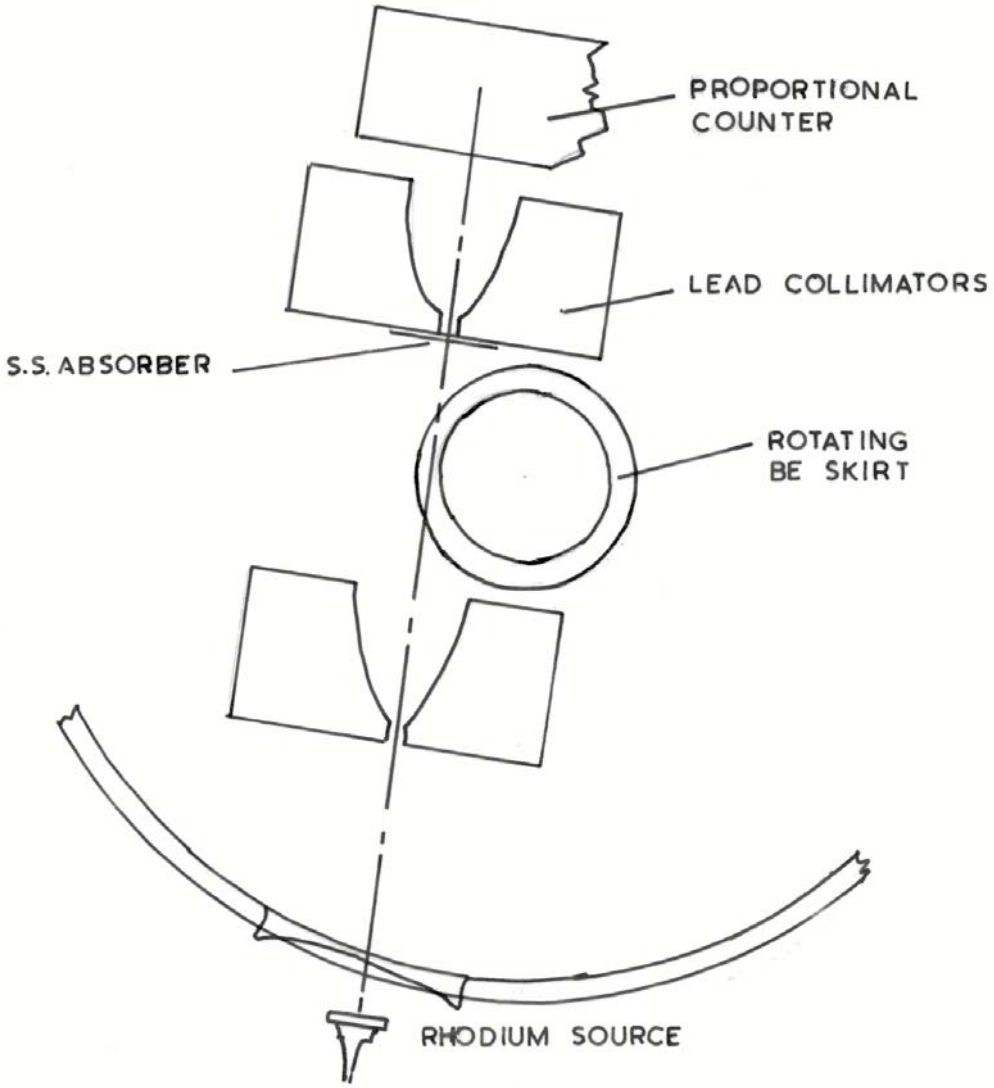
PROPORTIONAL
COUNTER
LEAD COLLIMATORS
S.S. ABSORBER
ROTATING
BE SKIRT
RHODIUM SOURCE

FIGURE 6.23